Research Square

Preprints are preliminary reports that have not undergone peer review.
They should not be considered conclusive, used to inform clinical practice,
or referenced by the media as validated information.

Influence of volume shrinkage and axial force variation on the rheological characterization of waxy oils

André da Silva Guimarães
Universidade Federal do Rio de Janeiro
Thiago Oliveira Marinho
Petrobras
Pedro Tavares Pereira
Universidade Federal do Rio de Janeiro
Príamo Albuquerque Melo
Universidade Federal do Rio de Janeiro
Roney Leon Thompson
Universidade Federal do Rio de Janeiro
Marcio Nele
nele@eq.ufrj.br
Universidade Federal do Rio de Janeiro

Research Article

Keywords: Waxy oil, axial force, rheology artifact, void formation, volume shrinkage

Posted Date: November 25th, 2026

DOI: https://doi.org/10.21203/rs.3.rs-11761832/v1

License: This work is licensed under a Creative Commons Attribution 4.0 International License.
Read Full License

Additional Declarations: No competing interests reported.

Influence of volume shrinkage and axial force variation on the rheological characterization of waxy oils

André da Silva Guimarães[1,2], Thiago Oliveira Marinho[3†], Pedro Tavares Pereira[1†], Príamo Albuquerque Melo[1†], Roney Leon Thompson[4†], Marcio Nele[1*†]

[1*]Programa de Engenharia Química (PEQ/COPPE), Universidade Federal do Rio de Janeiro, Avenida Horácio Macedo - Bloco G, Rio de Janeiro, 21941-598, Rio de Janeiro, Brazil.
[2]Department of Chemical Engineering, Faculty of Natural Sciences, Norwegian University of Science and Technology, Sem Sælands vei, Trondheim, 7034, Trøndelag, Norway.
[3]EDIVIT Corporate Office, Petrobras, Av. Nossa Sra. da Penha, Vitória, 29057-550, Espírito Santo, Brazil.
[4]Programa de Engenharia Mecânica (PEM/COPPE), Universidade Federal do Rio de Janeiro, Avenida Horácio Macedo - Bloco G, Rio de Janeiro, 21941-598, Rio de Janeiro, Brazil.

*Corresponding author(s). E-mail(s): nele@eq.ufrj.br;
Contributing authors: asguimaraes@peq.coppe.ufrj.br; thiagomarinho333@gmail.com; pedro.pereira@peq.coppe.ufrj.br ; melo@peq.coppe.ufrj.br; rthompson@pem.coppe.ufrj.br;
†These authors contributed equally to this work.

Abstract

Accurate measurement of rheological properties of gelled waxy oils, particularly the yield stress (τ_y), is essential for pump sizing and for mitigating line-blockage risk. However, laboratory measurements are often affected by gelation and volume shrinkage-related artifacts. In this scenario, waxy model oils containing 5 to 10 wt% of wax were evaluated under oscillatory rheology. Temperature ramps (0.5 to 2 °C·min^{-1}), along with time and amplitude sweeps at 4 °C, were performed using sandblasted cone-and-plate, grooved Couette, and serrated parallel-plate

geometries. Firstly, it was observed that wall slip had a stronger effect in cone-and-plate rather than Couette geometry due to the impact of axial force reduction during cooling. However, further studies showed kinks in the moduli data during cooling and an abrupt inversion in the axial force profile, due to the formation of a visually observed cavity in the sample at concentrations above 7.5 wt%. Poor test repeatability and strong dependence on the preparation and initial test temperature were also observed. Moreover, the moduli showed non-monotonic behavior, coupled with axial stress relaxation at 4 °C. The results suggest that axial force drop and relaxation strongly impact rheology measurements and should not be disregarded.

Keywords: Waxy oil, axial force, rheology artifact, void formation, volume shrinkage

1 Introduction

Waxy oils are complex fluids that have been intensively studied in rheology [1–3]. The in-depth investigation of this material is primarily attributed to its economic importance in flow assurance [4–6]. Moreover, multiple rheological behaviors and experimental artifacts have prompted researchers to deepen their understanding of waxy oil gelation and breakage [3, 7–10]. However, obtaining reliable rheological measurements depends on properly interpreting and mitigating test artifacts [11].

The main challenges encountered in testing waxy oil rheology include sample evaporation, wall slip, shear banding, and volume shrinkage [3, 8, 9, 12, 13]. In addition, the test results are also affected by sample composition, shear history, and thermal history [3]. In this scenario, waxy model oils are widely used to simulate crude oil properties and build understanding of the material using a simpler composition. For the oil phase, materials include single alkanes, such as dodecane, or combinations of linear, cyclic, and branched hydrocarbons, such as mineral oils and petrolatum [14–18]. Single alkanes and polydisperse waxes, including linear and branched alkanes, are also applied for the solid phase [15, 16, 19]. It is worth noticing that combinations of mineral oil and commercial waxes still contain many compounds.

Material evaporation artifacts can be reduced by heating the sample to 80 °C for 1 or 2 hours, thereby inducing volatile losses prior to testing [12]. Moreover, solvent traps and geometry covers are widely used to prevent sample loss and water condensation on the geometry at low temperatures [12]. Furthermore, the sample preparation protocol is also important for reducing thermal and shear-history effects and increasing test repeatability.

Wall slip is also an extensively studied problem for waxy oils. The use of geometries with sandblasted, serrated, and grooved surface finishing, and also vane geometries, is strongly advised in the literature [8, 9, 20–22]. However, cohesive and adhesive failures can occur in field pipelines, depending on the tube characteristics [21, 23]. Cone-plate geometries are preferable for many materials due to the constant stress distribution along the geometry radius. However, particle and cluster sizes should be considered when investigating the breakage process, as the gel changes from a network material

to a suspension [24]. In this scenario, grooved Couette geometries can also be applied [8]. Meanwhile, large sample volumes are required, and thermal resistance increases, delaying sample cooling and heating. On the other hand, volume shrinkage issues have driven the use of parallel plates to compensate for sample contraction and prevent cavity formation, usually referred to as voids [9].

Sample contraction decreases the axial force in materials such as resins, agar gels, and waxy oil gels [9, 25, 26]. Axial force measurement can be used to determine the gelation temperature. Moreover, in a constant-axial-force protocol, the variation in gap can be used to calculate the amount of shrinkage [25, 27]. In Shinde and Kumar [9], a constant axial force protocol showed better test repeatability than a constant gap experiment. Using a fixed gap across different aging times, the authors observed a decrease in material yield stress, whereas a constant-axial-force protocol did not show this effect. It is worth noting that in the fixed-gap protocol, when the sample was held isothermally at 4 °C, a gradual axial force release was observed. Therefore, testing the sample under different aging times was intended to measure yield stress at different axial force levels. As a consequence, yield stress varied over time. Moreover, the axial stress release during the isothermal time was attributed to sample detachment from the geometry.

For agar gels, Mao et al. [26] observed a non-monotonic behavior for the storage modulus after cooling. During the test, the thermal compensation mechanism for the geometry was deactivated. During cooling, the axial force decreased due to gelation, while the storage modulus increased. In contrast, the storage modulus peaked and then decreased during the isothermal period at a low temperature, while the axial force increased non-monotonically. Similarly to Shinde and Kumar [9], the observed axial force increase during isothermal time after sample cooling was attributed to sample detachment from the geometry. However, comparing the constant gap and constant normal force protocols revealed a lower storage modulus in the latter. The constant axial force protocol can compensate for contraction and increase test repeatability. Meanwhile, volume shrinkage in waxy oils is accompanied by void formation [28–30]. Aside from lateral contraction, voids can form within the bulk, leading to non-homogeneous materials. Moreover, since the sample is compacted to rearrange over the plates, the nature of the test is not quiescent.

From this perspective, this work aims to revisit volume shrinkage artifacts in rheometry of waxy oils. For this, a model waxy oil was used as the object of study in oscillatory tests. First, wall slip is demonstrated in a sandblasted cone-plate geometry compared with a grooved Couette geometry. The effects of concentration and cooling rate on the sample properties are then highlighted. Moreover, volume shrinkage artifacts, including void formation, localized breakage, and the non-monotonic behavior of storage modulus at 4 °C, are investigated. To the best of our knowledge, this is the first time that volume shrinkage artifacts have been studied from the perspective of oscillatory rheology for waxy oils. Furthermore, studies on this subject for waxy oils remain scarce in the literature.

2 Literature review

2.1 Volume shrinkage on waxy oils

The gelation of waxy oils is governed by the crystallization of n-alkanes in solution. As the fluid cools, the solubility of these molecules decreases, leading to nucleation and crystal growth organized in a three-dimensional crystalline network. This microstructure confers elastic properties and a pronounced dependence on thermal and mechanical histories [2].

During the sol-gel transition, specific volume decreases significantly, a phenomenon known as thermal shrinkage. This contraction results from both the natural increase in liquid hydrocarbon density at lower temperatures and the liquid-to-solid phase transition of paraffins, which are denser in their crystalline state [9]. In rheological tests in parallel and cone-plate geometries, volume shrinkage generates axial tension that pulls on the measuring surfaces due to contraction and void formation [9, 20]. Chala et al. [30] provide a consistent review of this subject.

However, thermal shrinkage does not necessarily result in voids within the waxy oil itself. As long as the reduction in volume can be accommodated by flow and redistribution of the material, shrinkage does not necessarily produce internal cavities. However, as crystallization proceeds and an interconnected gel network develops, such redistribution becomes increasingly restricted. Continued reduction in specific volume may then result in localized void formation within the gel [9, 31].

Among the quantification methods for void formation, Magnetic Resonance Imaging (MRI) has been extensively applied by Chala and co-workers [30, 32–37] to visualize and quantify cavities in gelled waxy crude oils in a small-scale pipeline. In these studies, T2-weighted images were used to distinguish the oil from gas-filled regions, allowing the void area to be quantified at different cross-sections and subsequently used to estimate its volume and spatial distribution.

Early investigations showed that void formation depends on thermal history. Chala et al. [32] reported total void fractions of approximately 7-12% and observed that the radial distribution of voids varied with cooling conditions, with faster cooling associated with larger void volumes near the pipe wall and slower cooling with a greater contribution from the pipe core. Subsequent experiments considering different combinations of initial and final cooling temperatures reported variations in void fraction under different thermal histories [33]. However, the isolated effect of the initial temperature above the wax appearance temperature was later reported to be relatively small [35].

Dynamic cooling conditions were also associated with differences in void formation and spatial distribution. Chala et al. [34] reported variations in both the total void volume and the radial distribution with flow rate, with lower flow rates associated with larger total void fractions and a greater contribution near the pipe wall. More recently, Chala and Sulaiman [38] compared dynamic and static cooling conditions and reported a more uniform axial distribution under the dynamic conditions investigated, whereas statically cooled samples showed greater variability along the pipe, particularly at lower final temperatures. Although the latter study refers to the analysis as a “void

size distribution", the reported distributions are based on the total void area measured in each cross-sectional MRI image rather than the size of individual cavities.

An important limitation of this technique, as implemented by the authors, is that the test section must be removed from the cooling system before scanning, thereby allowing heat exchange with the surroundings and potentially reducing the void fraction prior to image acquisition. Chala et al. [36] directly investigated this effect and observed a decrease in total void fraction from 7.16% to 6.09% over a 50 min waiting period, with the largest changes occurring at shorter waiting times. Therefore, although MRI provides detailed spatial information on void distribution, the time elapsed between cooling and scanning must be controlled when quantitative void fractions are compared.

In addition to MRI, Electrical Capacitance Tomography (ECT) has been investigated as an alternative technique for the online monitoring of waxy crude oils. ECT measures the capacitance between multiple electrodes distributed around an insulating pipe, which varies according to the permittivity distribution within the sensing region. After calibration, the measured capacitances are used in an inverse reconstruction procedure to obtain cross-sectional maps of the permittivity distribution, from which the spatial distribution and fraction of different phases can be estimated [39].

The first applications of ECT to waxy crude oils were primarily exploratory. Shafquet et al. [40, 41] investigated sensor configurations, calibration procedures, and image-reconstruction approaches, providing the initial basis for applying the technique to waxy crude oils during cooling. A subsequent study developed a more quantitative implementation using a dual-plane ECT sensor to monitor statically cooled waxy crude oil online [42]. The capacitance measurements were reconstructed using the linear back projection algorithm and the resulting images were processed by thresholding to estimate the void fraction. The estimated void fraction increased as cooling progressed, reaching approximately 11-14% at 10 °C in both measurement planes.

However, quantitative interpretation of ECT results depends on the calibration and image reconstruction procedures adopted. The linear back projection method used in these studies enables rapid image reconstruction, but relies on an approximate solution of the inverse problem, and therefore provides essentially qualitative images. Quantitative estimates of void fraction thus require additional processing and prior information to relate the reconstructed permittivity distribution to the phase distribution [43].

In general, MRI and ECT provide complementary approaches to characterizing voids in waxy crude oils. Both are non-destructive techniques and provide spatial information on void distribution. MRI provides a more detailed spatial characterization. However, the sample must be removed from the cooling system before scanning, which may affect the measured void volume [36]. In contrast, ECT allows for online measurements and provides rapid, non-ionizing monitoring, although the spatial detail obtained strongly depends on the reconstruction procedure employed [43, 44].

Although the techniques discussed were applied to pipeline measurements, it is important to reemphasize that the presence of voids affects the mechanical properties of waxy oil gels. Therefore, the characterization of contraction and void formation is an important subject in rheological measurements, since the conditions imposed during

cooling may influence the gel's structure. In this scenario, Shinde and Kumar [9] investigated this effect by comparing constant-gap and constant-normal-force protocols during cooling with a subsequent yielding of a model waxy oil gel. Under constant-gap conditions, contraction below the gelation temperature generates a tensile normal force while the fixed plate prevents the sample from axial contraction, leading to the formation of voids within the crystal network. On the other hand, under the constant-normal-force protocol, the normal force is maintained close to zero by allowing the upper plate to move downward as the gel contracts. The resulting reduction in gap partially compensates for volume contraction, minimizing void formation and promoting a more homogeneous gel structure.

The comparison between these protocols revealed two important consequences of void formation. First, critical-stress measurements obtained under constant-gap conditions showed poorer repeatability. The authors attributed this variability to the dynamic nature of void formation, as void size and location cannot be controlled, and different void distributions yield mechanically distinct gel structures. In addition, the critical stress measured under constant-gap conditions was systematically lower than that obtained when contraction was compensated through the constant-normal-force protocol. This difference became progressively larger as the final cooling temperature decreased and the wax concentration increased, which the authors attributed to greater void formation under constant-gap conditions [9]. Thus, void formation not only reduces the gel's apparent mechanical strength but also introduces additional variability in its rheological characterization. In this scenario, it is important to reevaluate the suitability of the geometries used in rheological tests.

2.2 Influence of the geometries on the measurements

Cone-and-plate geometries are often preferred for fundamental studies due to the constant stress distribution along the radius [45]. However, in waxy oils, the small truncation gap of the cone (often around 50 μm) can be comparable to the size of wax crystal clusters, generating flow disturbances [46]. Gap size requirements for a proper yield stress measurement are discussed by Japper-Jaafar et al. [47].

Grooved concentric cylinders (GCC) geometry has proven to be more effective in reducing experimental noise and preventing sudden shifts in cooling curves. By fully enclosing the rotor, the probability of total geometry detachment is lower than in open parallel plate systems. However, GCC requires larger sample volumes and consequently has increased thermal resistance, which can lead to thermal delays and internal gradients [8].

To tackle axial force and gel contraction, serrated parallel plates provided the most robust performance under the tested conditions. The serrated finish provides mechanical interlocking that suppresses wall slip more effectively than sandblasted surfaces [8]. More importantly, parallel plate geometry enables dynamic vertical adjustment of the rotor to compensate for volume contraction, an essential feature for controlled axial force protocols [9].

The implementation of a constant axial force protocol ($F_N \sim 0$ N) aims to maintain continuous contact between the geometry and the sample without exerting excessive compression or allowing traction. In this mode, the rheometer head moves upward or

downward as the material expands or contracts. By keeping the axial force near zero, the equipment prevents the gel from being pulled axially during crystallization, impeding internal void formation and premature fractures, leading to a more homogeneous gel network and mitigating uncertainties in yield stress measurements associated with thermal contraction [9, 28].

The loss of light components through evaporation alters the relative wax concentration, artificially inflating G' and τ_y values over time. The use of solvent traps and geometry covers is required. In addition to mitigating mass loss, these covers prevent condensation of water on the geometry at low temperatures (e.g., 4 °C), which could act as a lubricant and facilitate wall slip. Figure 1 exemplifies the water condensation issue in a Couette geometry at 4 °C.

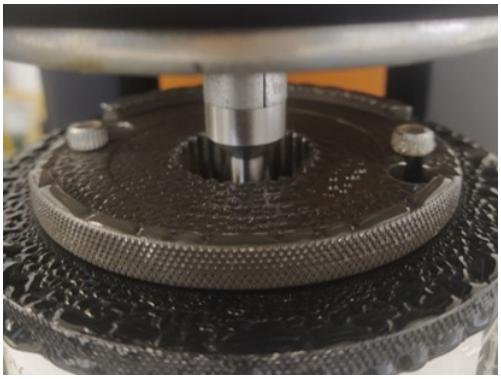


Fig. 1 Water condensation in a Couette geometry at 4 °C.

3 Methodology

3.1 Sample description and preparation

The waxy model oils were prepared using Exxsol D60 as the oil phase and the predominant macrocrystalline wax SASOL 5405. The wax has a melting point range from 53 to 55 °C. Exxsol D60 comprises linear, branched, and cyclic alkanes in the range of 10 to 13 carbons. Moreover, the oil density ranges from 774 to 809 kg·m^{-3} at 15 °C. The samples were prepared by dissolving the waxes in the oil using a heated magnetic stirrer (Arex Digital Pro, Velp Scientifica, Italy) for 1 hour. The preparation temperature varied from 60 to 80 °C, and the stirring speed was 400 rpm. After preparation, samples were stored at room temperature and heated to the initial test temperature for 1 hour prior to each rheological test.

3.2 Sample characterization

3.2.1 Wax and oil composition assessment by Gas Chromatography (GC)

Gas chromatography (GC) tests with a mass spectrometer (MSD) and a flame ionization detector (FID) were performed to assess the sample composition. The tests were conducted on an Agilent 7890B instrument. The chromatograph was equipped with a 7693A injector, a 5977B MSD detector, and a DB-1HT capillary column with a 30 m length, 0.25 mm diameter, 0.1 μm film thickness, and helium as the carrier gas. The protocols were based on Ruwoldt et al. [48] and Savasdipol et al. [49] and are fully described in Appendix A. The AMDIS [50] software was used to support peak deconvolution and identification using the embedded alkanes mass spectra library, and OriginPro 2026 was used for the peak integration procedure.

3.2.2 Crystallization behavior by Differential Scanning Calorimetry (DSC)

DSC tests were conducted on a Q2000 differential scanning calorimeter (TA Instruments, USA) to characterize the thermal behavior of the material. The experiments were performed using Tzero aluminum hermetic pans with a sample mass of about 15 mg. The thermograms of pure wax and oils are available in Appendix B. For the model waxy oils, after previous solubilization in the circulating oven, the sample was weighed in the pans and placed in the equipment. The thermal protocol consisted of equilibrating the sample at 50 °C and cooling it at 0.5, 1, and 2 °C·min^{-1} from 50 to -40 °C. Moreover, after equilibration at -40 °C, the samples were heated to 50 °C at the same rates. Additionally, the samples were isothermally evaluated for 1 hour at 4 °C under the same initial protocol (50 to 4 °C at the specified cooling rates). The wax appearance and disappearance temperatures, WAT and WDT, were obtained from the tangent method. The Chen et al. [37] method was applied to account for the mass fraction of crystallized wax.

3.3 Rheometry experimental setup

The rheological tests were conducted using a Physica McR 301 rheometer from Anton Paar. Before each test, the sample was preheated for at least 1 hour in a circulating oven (VENTI-Line Prime, Avantor, USA) at the same initial test temperature to ensure repeatability. Initial temperatures of 50 and 60 °C were investigated. Then, the sample was homogenized at 400 rpm for 5 minutes at the same temperature using a magnetic stirrer. The glass pipettes and syringes used to place the sample were kept in the oven at a constant temperature for 1 hour to prevent crystallization on cold surfaces during sample manipulation. Moreover, the rheometer geometry was preheated to the initial temperature, and the sample was held at this temperature for 5 minutes before each test. For all tests conducted in the cone-and-plate and parallel-plate geometries, an upper-heated Peltier system model H-PTD200 was also used. For Couette geometry, a solvent cover was used instead.

The oscillatory rheology data were evaluated based on the rheometer minimum torque limit. In this regard, the methodology of Ewoldt et al. [11] was applied. The minimum measurable values for moduli, applied to both the storage and loss moduli, were calculated based on the equipment's precision and geometric characteristics.

Equation 1 gives the expression for the minimum readable modulus, G_{min}. F_τ is the stress geometry factor, $M_{min,osc}$ represents the minimum torque for oscillation, and γ is the strain amplitude.

$$G_{min} = \frac{F_\tau M_{min,osc}}{\gamma} \tag{1}$$

Data on mineral oil rheology is available in Appendix C.

3.4 Wall slip analysis in cone and plate and grooved Couette geometry

In this study, the samples were prepared at 60 °C, and the model waxy oils were cooled from 50 to 4 °C. The oscillatory cooling process was performed in a 40 mm sandblasted cone-and-plate (CP) geometry with an angle of 2° combined with a sandblasted lower plate and an upper heated Peltier plate (truncation gap = 57 μm, cone rugosity = 6.25 μm). The sample concentration and the cooling rate were set as 5 wt% of wax and 1.5 °C·min^{-1}, respectively. The model waxy oil was cooled under a fixed strain amplitude and frequency, as specified in Table 1. Tests 1-4 represent the CP geometry tests. The gelation experiments were followed by an oscillatory amplitude strain sweep from 0.01 to 10 % with the same frequency applied during cooling. The amplitude sweep aimed to determine whether the applied strain amplitude falls within the linear viscoelastic regime. Moreover, the yield stress was defined as the stress peak in the stress amplitude curve as a function of strain amplitude.

Table 1 Test conditions for wall slip analysis (CP ∴ Cone and plate; GCC ∴ Grooved concentric cylinders).

Test	Initial wax concentration (wt%)	Cooling rate (°C·min^{-1})	Strain amplitude (%)	Frequency (Hz)	Geometry
1	5	1.5	0.1	0.2	CP
2	5	1.5	0.1	1.0	CP
3	5	1.5	0.04	0.2	CP
4	5	1.5	0.04	1.0	CP
5	5	1.5	0.04	0.2	GCC

In addition, to evaluate wall-slip issues in a different setup, a cooling process test was also performed in a DIN grooved Couette geometry (GCC) (bob diameter = 26.660, bob length = 40 mm, cup diameter = 28.917 mm). In this regard, Test 5 (c.f. Table 1) was performed with the same test conditions as Test 3. With the exception that the strain amplitude was extended to 100 % to capture the stress amplitude peak and modulus crossover properly.

3.5 Effect of the initial wax mass fraction and cooling rate on the rheological properties in grooved Couette geometry

The effect of wax concentration was assessed by comparing samples behavior under cooling at 1.0 °C·min^{-1} and the strain amplitude sweep for the 5, 7.5, and 10 wt% concentrations. Similarly, the effect of the cooling rate was investigated for the 7.5 wt% sample at 0.5, 1.0, and 2.0 °C·min^{-1}. A cooling rate of 2 °C·min^{-1} was chosen instead of 1.5 °C·min^{-1} to space the data and better capture the variable effect. All tests were performed applying a fixed frequency of 0.2 Hz and a fixed strain amplitude of 0.02 % (within the linear viscoelastic region). The temperature ramp tests were followed by a strain amplitude experiment at 0.2 Hz from 0.01 to 100 %. A summary of the experiments is shown in Table 2, covering Tests 1 to 5. The tests at 7.5 wt% and 1.0 °C·min^{-1} were performed in triplicate to evaluate the test repeatability. In this section, the samples followed the previously applied sample thermal protocol.

Table 2 Test conditions for cooling rate and initial wax mass fraction analysis.

Test	Initial wax concentration (wt%)	Cooling rate (°C·min^{-1})	Strain amplitude (%)	Frequency (Hz)	Geometry
1	5	1	0.02	0.2	GCC
2	7.5	1	0.02	0.2	GCC
3	10	1	0.02	0.2	GCC
4	7.5	0.5	0.02	0.2	GCC
5	7.5	2.0	0.02	0.2	GCC

3.6 Analysis of volume shrinkage-induced artifacts in grooved Couette geometry

In this study, the tests were performed using the grooved Couette geometry. Except for the tests in Section 3.6.4, all samples were prepared at 60 °C. As previously described, samples were stored at room temperature and heated to the test temperature prior to each test. Moreover, the sample was cooled from 50 to 4 °C. The cooling rate applied was 1 °C·min^{-1}.

3.6.1 Onset of void formation and local failure

The cooling protocol, followed by the strain amplitude sweep, was also performed for 8 and 9 wt% samples. The tests were conducted under 0.02 % of strain amplitude at 0.2 Hz during the temperature ramp, and ranging from 0.01 to 100 % at 0.2 Hz in the strain amplitude sweeps.

In addition, a test for a 10 wt% sample was recorded using a 16 MP Samsung M15 camera to track void formation and sample breakage. The test was conducted at 1 Hz. As discussed in the following sections, the data sampling resolution could be enhanced by increasing the frequency from 0.2 Hz to 1 Hz. Furthermore, stress-relaxation effects

are expected to decrease at higher frequencies. Tests 1 to 3 in Table 3 summarize the experimental conditions for this section.

Table 3 Test conditions for volume shrinkage artifacts study in grooved Couette geometry.

Test	Initial wax concentration (wt%)	Cooling rate ($°C \cdot min^{-1}$)	Strain amplitude (%)	Frequency (Hz)	Geometry
1	8	1	0.02	0.2	GCC
2	9	1	0.02	0.2	GCC
3	10	1	0.02	1	GCC
4	5	1	0.02	0.2	GCC
5	7.5	1	0.02	0.2	GCC
6	10	1	0.02	0.2	GCC
7	10	1	0.02	0.2	GCC
8	10	1	0.04	0.2	GCC
9	10	1	0.02	1	GCC
10	10	1	0.04	1	GCC

3.6.2 Sample aging at 4 °C

The storage and loss modulus variation at 4 °C was also evaluated for the 5.0, 7.5, and 10 wt% samples. The model waxy oils were cooled under a fixed strain amplitude of 0.02 % at 0.2 Hz. Then, the samples were kept under the same oscillatory conditions for 1 hour at 4 °C. Lastly, a strain amplitude sweep was performed at 0.2 Hz, ranging from 0.01 to 100 %. Tests 4 to 6 describe the experimental conditions in Table 3.

3.6.3 Effect of the oscillation parameters

In this study, the samples were also prepared at 60 °C. 10 wt% samples were cooled and subjected to an amplitude sweep under the same thermal conditions as in the previous section, without isothermal time. Frequencies of 0.2 and 1 Hz, and strain amplitudes of 0.02 and 0.04 % were investigated, according to Tests 7 to 10 as shown in Table 3.

3.6.4 Effect of the sample preparation temperature on the test repeatability

This study evaluated the effects of preparation and initial temperature on test repeatability during sample aging. In the first part of the study, a 10 wt% sample was prepared and evaluated fresh and after 3 days. Aged samples were stored at room temperature and pre-heated at the initial test temperature for 1 hour prior to the tests. The dissolution temperatures used in sample preparation were 60, 70, and 80 °C. For the fresh sample, the cooling process in the rheometer started at 50 °C. After 3 days, the sample was tested starting at 50 °C and 60 °C. The test conditions for the cooling process were 0.02 % of strain amplitude and a frequency of 1 Hz. For the strain amplitude sweep, a strain range of 0.01-100 % and a frequency of 1 Hz were defined. Moreover,

the effect of sample aging on test repeatability was evaluated for a 7.5 wt% sample prepared at 80 °C. The tests were performed for the fresh sample and after 3 and 7 days. Before the strain sweep, the sample was kept under oscillation for 1 hour at a fixed temperature of 4 °C. Table 4 summarizes the test conditions.

Table 4 Preparation and initial temperature for the repeatability tests under sample aging.

Test	Preparation temperature (°C)	Initial test temperature (°C)	Sample age	Concentration (wt%)
1	60	50	Fresh	10
2	60	50	3 days	10
3	60	60	3 days	10
4	70	50	Fresh	10
5	70	50	3 days	10
6	70	60	3 days	10
7	80	50	Fresh	10
8	80	50	3 days	10
9	80	60	3 days	10
10	80	50	Fresh	7.5
11	80	50	3 days	7.5
12	80	50	7 days	7.5

3.6.5 Sample aging in parallel plate geometry

In this study, a 7.5 wt% waxy model oil prepared at 80 °C and the pure mineral oil were investigated. For this, a 75 mm serrated parallel plate combined with an upper heated Peltier plate were used. The gap between plates was set to 0.5 mm. Besides, the thermal protocol consisted of cooling the sample from 60 to 4 °C at 1 °C·min^{-1} and holding it at 4 °C for 1 hour. In this scenario, both a quiescent and an oscillatory protocol were applied to the 7.5 wt% waxy oil, and the quiescent protocol was also applied to the mineral oil. Under oscillation, a strain amplitude of 0.02 % and a frequency of 1 Hz were employed. At the end of the isothermal period, a strain sweep from 0.01 to 100 % at 1 Hz was applied in both scenarios. Moreover, for parallel plates, the sample was pre-sheared for 5 min at 5 s^{-1} before all tests.

4 Results

4.1 Sample characterization

4.1.1 Composition assessment by Gas Chromatography (GC)

Analysis of GC-MS and FID chromatograms identified alkanes ranging from 10 to 13 carbons in the mineral oil, in accordance with the manufacturer's specifications. The amount of linear alkanes was measured as 33 % using FID chromatogram. For the wax, a distribution from 19 to 36 carbons was identified, with an amount of 81 % of linear alkanes. This result is in accordance with the literature that indicates a

range from 78 to 84.6 % of linear alkanes [16, 48]. It is important to highlight that the carbon number distribution may be batch-dependent. TIC and FID chromatograms are available in Appendix A.

Figure 2 displays the linear and non-linear alkanes distribution within the wax (a) and mineral oil (b). Non-linear alkanes comprise cyclic and iso-alkanes.

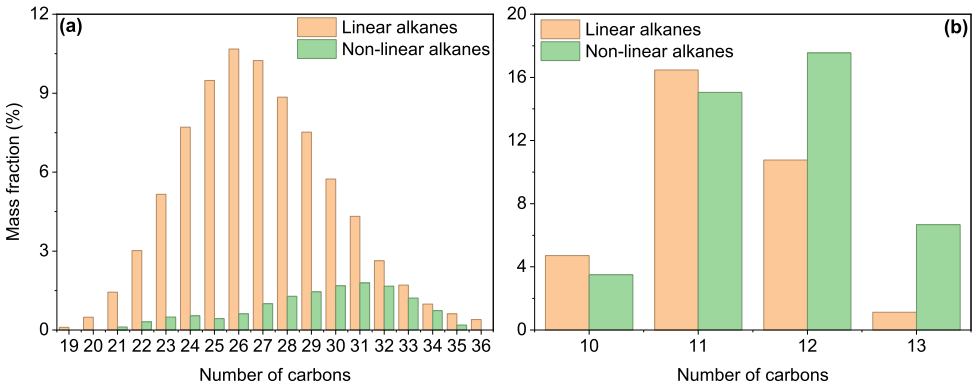


Fig. 2 Wax (a) and mineral oil (b) mass fraction as a function of carbon number.

4.1.2 Crystallization behavior by Differential Scanning Calorimetry (DSC)

The WATs and WDTs obtained for the waxy model oils are shown in Table 5. The WAT varied by 0.5 °C over the cooling rate range studied for the oil containing 7.5 wt%. In addition, the WDT displayed a 2.6 °C variation with the cooling rate for the same sample. These results show that the initial wax mass fraction had a greater effect on the WAT and WDT differences, which changed by 6.2 °C and 6.8 °C, respectively, compared to the 5 and 10 wt% samples.

Table 5 Wax appearance (WAT) and wax disappearance temperatures (WDT) for the waxy model oils.

Initial wax mass fraction (wt%)	Cooling rate (°C/min)	Wax appearance temperature (°C)	Wax disappearance temperature (°C)
5	1	17.5 ± 0.1	19.5 ± 0.3
7.5	0.5	22.0 ± 0.1	22.6 ± 0.3
7.5	1	21.8 ± 0.1	23.6 ± 0.3
7.5	2	21.5 ± 0.1	25.2 ± 0.3
10	1	23.7 ± 0.1	26.3 ± 0.3

The crystallized wax mass fraction profiles as a function of temperature obtained by Chen et al. [37] method are shown in Figure 3. The profiles display a negligible dependence on the cooling rate within the range investigated (Figure 3(a)) in comparison to the initial wax mass fraction (Figure 3(b)), suggesting thermodynamic limitation.

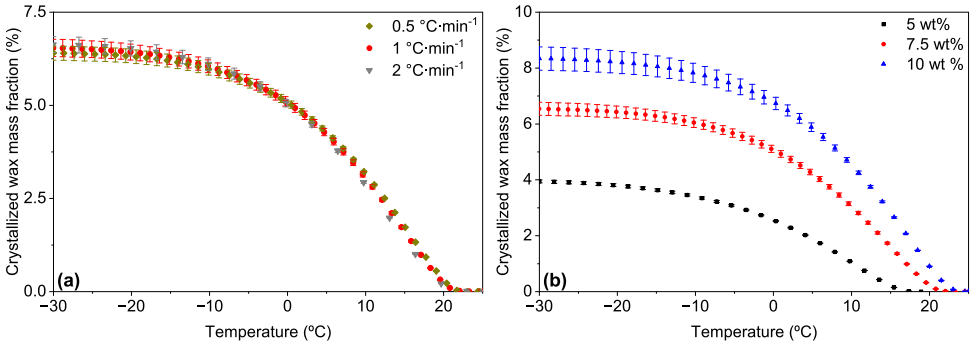


Fig. 3 Crystallized wax mass fractions as a function of cooling rate (a) and initial wax mass fraction (b).

Figure 4 displays thermograms for mineral oil (a) and for the 7.5 wt% waxy model oil (b) obtained by applying a temperature ramp until 4 °C followed by a 60 minutes isothermal protocol. In the first stage, when the mineral oil is cooled down (c.f. Figure 4 (a)), the heat flow measurement accounts only for heat capacity variations in the sample since no crystallization takes place for the mineral oil in this temperature range. After cooling is stopped, the heat flow baseline drops to zero and no heat flow is generated. In a similar manner, the waxy mode oil (c.f. Figure 4 (b)) displayed an instantaneous decrease in heat flow when the temperature reached 4 °C despite the heat flow peak. These tests revealed that crystallization ceased as the temperature was kept constant. Therefore, there is evidence that no isothermal crystallization occurs in the samples studied over the investigated range of cooling rates.

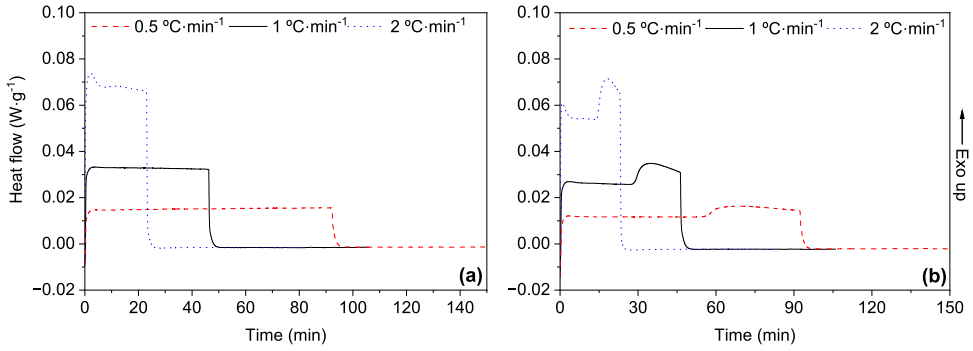


Fig. 4 Heat flow as a function of time for the mineral oil (a) and the 7.5 wt% waxy model oil (b).

4.2 Wall slip analysis in cone and plate and grooved Couette geometry

4.2.1 Temperature ramp and strain amplitude sweep in cone and plate geometry

To understand the gelation behavior of the sample and evaluate wall slip, the storage modulus, loss modulus, axial force, and stress amplitude were monitored during cooling. Figure 5 shows the moduli and stress amplitude results obtained for the cone and plate geometry, varying the frequency and strain amplitude.

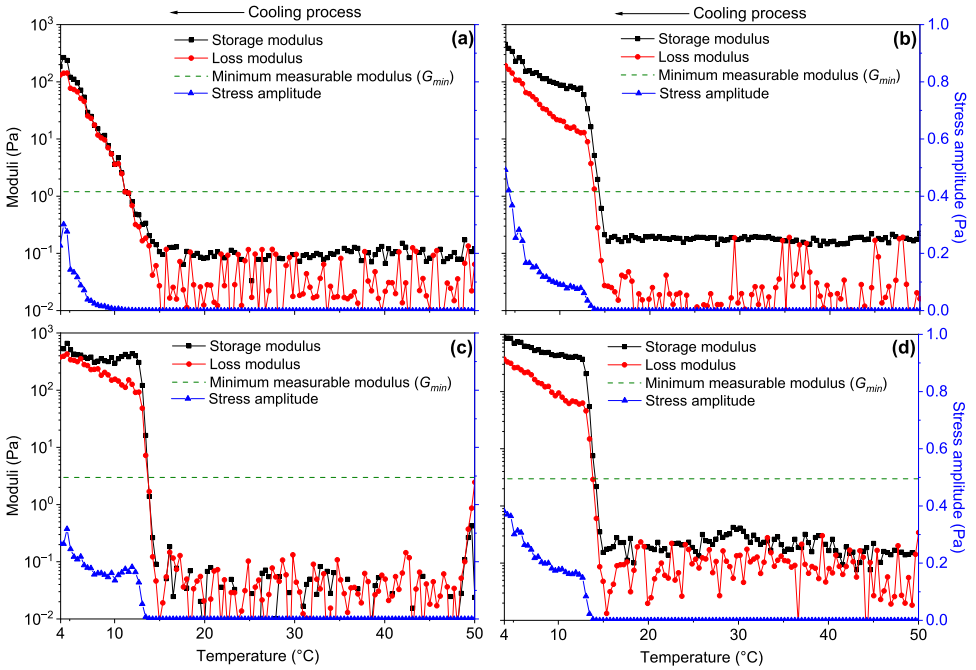


Fig. 5 Temperature ramps in cone and plate geometry for a 5 wt% waxy model oil at 1.5 °C·min^{-1} under: (a) 0.1% at 0.2 Hz; (b) 0.1% at 1 Hz; (c) 0.04% at 0.2 Hz; (d) 0.04% at 1 Hz.

Figure 5 (a) shows multiple crossovers between the storage and loss moduli due to the scattering of the data. This artifact hindered the proper determination of gelation temperature. However, a modulus onset was observed at 14 °C that corresponds only to 0.36 wt% of crystallized wax. On the other hand, in Figure 5 (b), the moduli crossover did not occur at 1 Hz, although an onset is observed at 15 °C (0.21 wt% of wax). In addition to the moduli onset, the curve shows an abrupt change in slope at 12.4 °C (0.63 wt% of wax). One of the main issues hindering crossover detection was that the transition occurred at a moduli value below the equipment's minimum torque limit, represented by G_{min}. In the figures, this limit is marked by the green full dashed line, corresponding to 1.2 Pa at 0.1% and 2.99 Pa at 0.04%. Concerning Figure 5 (c), for a strain amplitude of 0.04% and a frequency of 0.2 Hz, a crossover was observed

at 13.7 °C (0.41 wt%). However, for the same amplitude at 1 Hz, the crossover did not occur, as shown in Figure 5 (d). The multiple crossovers and the abrupt change in the slope of the curve after gelation highlight wall slip.

In addition to tests under cooling, amplitude sweeps at 4 °C were carried out as shown in Figure 6, the amount of wax crystallized at this temperature was about 2 wt%. Figure 6 shows that the storage and loss moduli increased in the 0.01% to 0.03% strain amplitude interval, which can result from a residual structuring effect at 4 °C. Accordingly, a well-defined linear viscoelastic region is not observed. Regarding the amplitude values applied, 0.1 % is out of the linear viscoelastic region, and values lower than 0.04 % are appropriate for the tests. In addition, subtle changes in the stress amplitude were observed in the curve peaks, consistent with interfacial slip or partial loss of mechanical coupling between the sample and the geometry. The yield stress, assumed here to be the peak in the stress amplitude, ranges from 2.3 to 4.3 Pa for the 5 wt% model waxy oil. Correspondingly, the strain amplitude at the peak was assumed to be the yield strain, which ranged from 0.28 to 0.45 %.

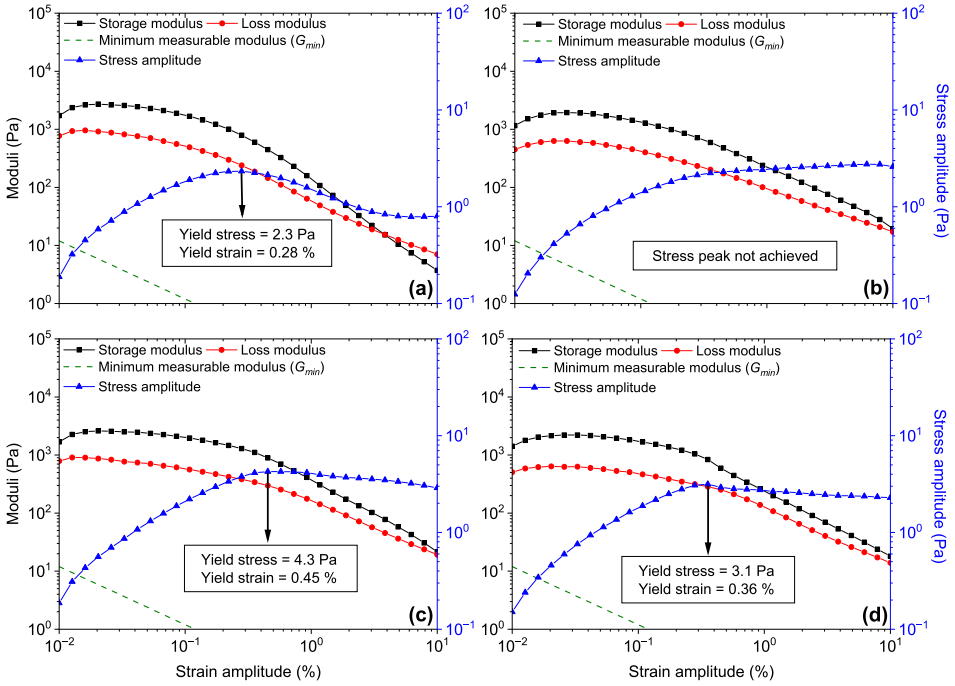


Fig. 6 Amplitude strain sweeps at 4 °C for a 5 wt% sample after temperature ramp under: (a) 0.1% at 0.2 Hz; (b) 0.1% at 1 Hz; (c) 0.04% at 0.2 Hz; (d) 0.04% at 1 Hz. The arrows indicate where the yield stress peaks were identified.

Wall slip can be increased due to axial force variation during the tests. During zero-gap calibration, the instrument sets the axial force to 0 N. When the sample is loaded, the equipment measures a small negative axial force (≈-0.06 N at 50 °C). The

measured value results from the force balance between hydrodynamic and capillary effects. According to Figure 7 (a), the axial force decreases linearly as a function of temperature before gelation, which occurs due to the thermal contraction of the sample. However, there is a more pronounced decrease in the axial force below 15 °C due to gelation and volume shrinkage. Comparatively, Figure 7 (b) shows that when crystallization started, the increase in axial force drop rate is not appreciable until at least 1 wt% of wax is solidified. Then the axial force starts to decrease faster and drops below -0.08 N. It is also important to highlight that the data for the axial force during gelation are also scattered. Moreover, the wall slip is facilitated by the downward pull of the sample over the geometry [9, 20, 26]. The model oil axial force curves in Figure 7 (a) are shown together with the pure oil axial force variation during cooling for comparison. Also, since the crystallized wax mass fraction was shown to have only a small variation with the cooling rate in the range studied (0.5 to 2 °C·min^{-1}), the data were interpolated to 1.5 °C·min^{-1} to get information on how axial force decreases as the solidified wax concentration increases.

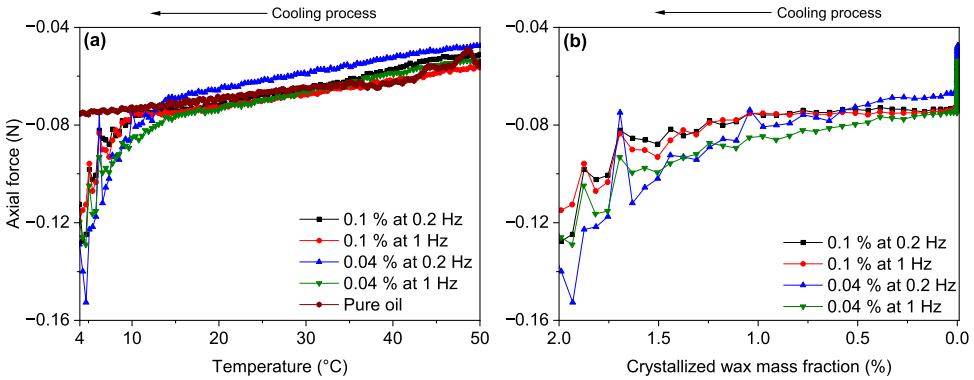


Fig. 7 Axial force variation during cooling on cone and plate geometry for a 5 wt% sample and pure oil at 1.5 °C·min^{-1} as a function of (a) temperature and (b) crystallized wax mass fraction.

4.2.2 Temperature ramp and strain amplitude sweep in grooved Couette geometry

Figure 8 shows the temperature ramp (a) and the amplitude strain sweep results at 4 °C (b) in the grooved Couette geometry (5 wt% sample at 1.5 °C·min^{-1}). In Figure 8 (a), a smoother growth of the storage modulus is observed compared to the cone and plate geometry. Moreover, no abrupt changes in slope occurred in the curves. On the other hand, due to the low solid concentration, the modulus crossover also occurred below the minimum torque limit. A difference in the moduli onset was also observed, occurring around 10 °C instead of 14 °C in the cone-and-plate geometry. This difference may highlight inertial thermal effects in the grooved Couette geometry, owing to the larger sample volume. Similar observations apply to the strain amplitude sweep tests, with the curve smooth and showing no abrupt changes. A comparison

between the storage modulus and the stress curves between the geometries is shown in Figure 9 (a) and (b), respectively.

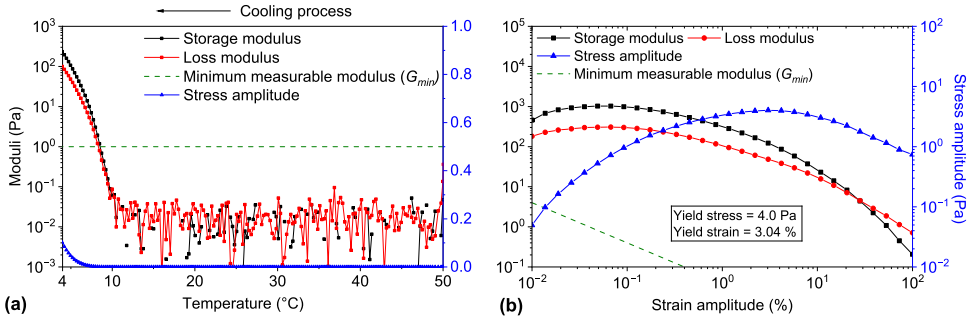


Fig. 8 (a) Temperature ramp and (b) amplitude sweep at 4 °C for 5.0 wt% sample cooled at 1.5 °C·min^{-1} in the grooved Couette geometry (0.04 % at 0.2 Hz).

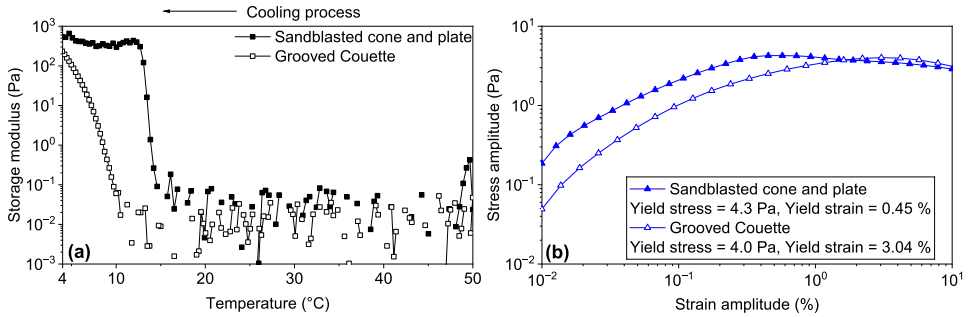


Fig. 9 Comparison between cone and plate and grooved Couette geometry for the (a) storage modulus during cooling and (b) stress amplitude during strain amplitude sweep (5 wt%, 1.5 °C·min^{-1}).

Figure 9 (a) compares the storage modulus behavior during cooling between geometries. The storage modulus increase for the cone-and-plate is steeper and marked by an abrupt change after the initial onset. In contrast, for grooved cylinders, the modulus increase is smoother. The stress amplitude curves are also compared, as shown in Figure 9 (b). It was observed that the qualitative behavior of the curves is similar until the peak is reached. Furthermore, the yield stress obtained was 4.3 Pa for the cone-and-plate geometry and 4 Pa for the cylinders and the corresponding values of yield strain were 0.45 % and 3 %, respectively.

By tracking the axial force during the tests, unlike the cone-and-plate, the initial sample loading leads to a small positive value (~0.16 N at 50 °C), as shown in Figure 10. In this case, buoyancy forces may also be relevant in the axial force balance. For the pure oil, the cooling process did not promote significant changes in the axial force (c.f. Figure 10(a)). However, for the 5 wt % sample, the contraction effect also leads to a decrease in axial force during gelation (~0.03 N). In this scenario, in comparison

to the cone and plate, the sample covers the bob, reducing the probability of sample detachment from the geometry. But, for higher concentrations of wax in the oil, the strong impact of axial force decrease in the sample can still be a source of test artifacts, as will be discussed in the next sections. Furthermore, Figure 10(b) shows how the axial force is impacted by the crystallized wax mass fraction. A significant decrease in the axial force is observed only when about 1.25 wt% of wax is crystallized.

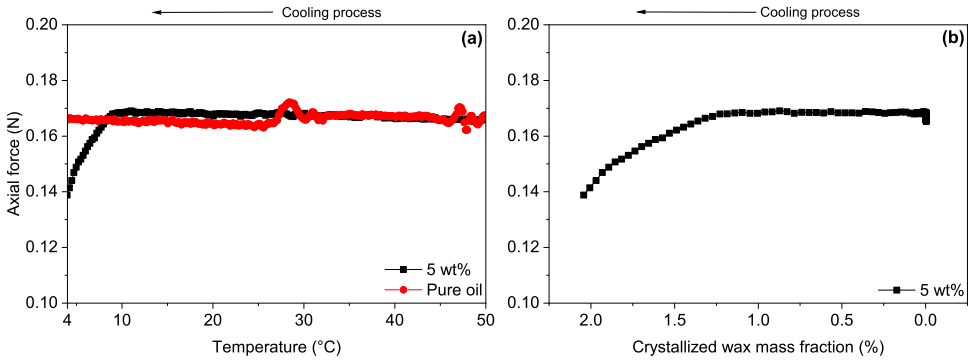


Fig. 10 Axial force behavior during cooling for the pure oil and the 5 wt% sample in the grooved Couette geometry with (a) temperature and (b) crystallized wax mass fraction.

4.3 Effect of the initial wax mass fraction and cooling rate on the rheological properties

In this section, the effects of the initial wax mass fraction and cooling rate on the rheology were evaluated using GCC geometry.

4.3.1 Effect of the initial wax mass fraction

Figure 11 shows the temperature ramp for 5, 7.5, and 10 wt% waxy model oils ((a) to (c), respectively), and a picture of the 10 wt% sample after the test (d).

The curves in Figure 11 (a) to (c) demonstrate an evident increase in the modulus crossover temperature corresponding to 9.5, 15, and 18 °C for 5, 7.5, and 10 wt% waxy model oils, respectively. The crystallized wax mass fraction at the gelation threshold was approximately 1.1, 1.6, and 1.7 wt%. The magnitude of the storage and loss moduli also increased with concentration. It is worth noticing that a kink in the storage modulus data was observed at 4.98 °C for the 7.5 wt % sample and 10.48 °C for the 10 wt % model waxy oil, corresponding to 4.2 and 4.4 wt% of crystallized wax, as highlighted by a yellow ellipse. Remarkably, a void was formed in the 10 wt% waxy model oil, illustrated in Figure 11 (d). Similar cavities have been reported in the literature [29, 33, 40, 42], usually referred to as a void. The phenomenon is attributed to volume shrinkage.

Besides the storage modulus kink artifact in the data, an abrupt inversion in the axial force curve was observed for the 7.5 wt% and 10 wt% samples, as shown in

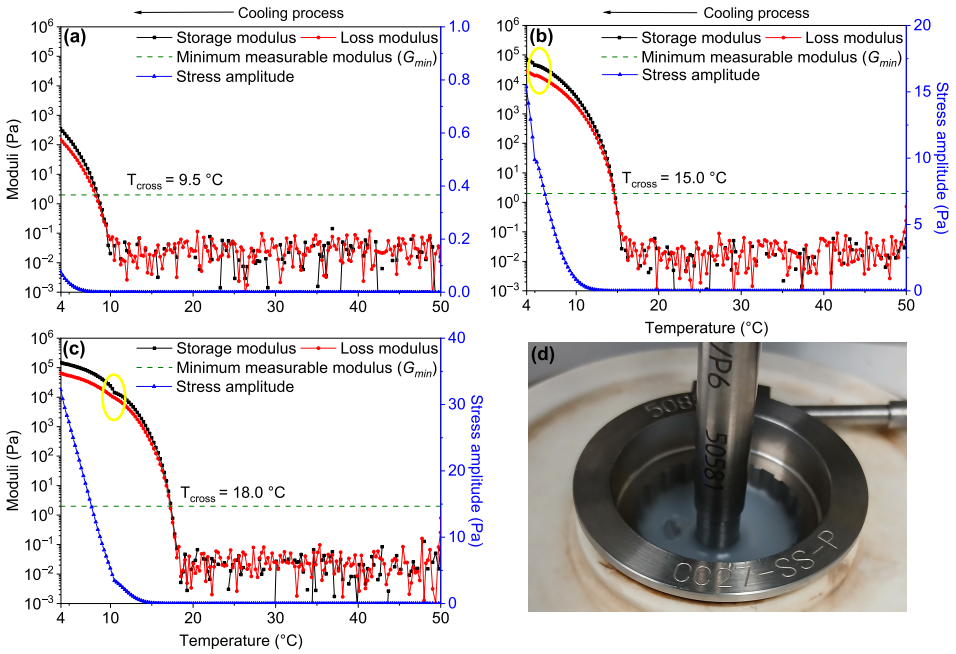


Fig. 11 Cooling process effect on moduli and stress amplitude for the waxy model oils containing 5 (a), 7.5 (b), and 10 wt% of wax at 1 °C·min^{-1} (c), and a 10 wt% sample picture after the test (d)(0.02 % of strain amplitude at 0.2 Hz).

Figure 12. The inversions in temperature occurred at 5.23 and 10.73 °C, respectively, denominated as T_{inv} (c.f. Figure 12(a)). The same limit was denoted as ϕ_{inv} for the crystallized wax mass fraction (c.f. Figure 12(b)). T_{inv} and ϕ_{inv} were characterized by a local minimum in the data and occur near to the storage modulus kink appearance. The green dotted circles in the figures highlight the inversion occurrences. Moreover, for the 5 wt% sample, the magnitude of the decrease in the axial force was not appreciable. For the 7.5 and 10 wt% model waxy oils, the minimum axial force was around -6 N. Interestingly, the 7.5 wt% sample did not exhibit visible void formation despite the appearance of a kink in the data and the observed curve inversion. Also, it is important to highlight that cavity formation makes the material non-uniform and can lead to localized breakage. Detailed aspects of volume shrinkage artifacts will be discussed in the following sections. More images of cavities formed in the following tests are available in Appendix D.

The results of the strain amplitude sweep tests are shown in Figure 13. The yield stress increased significantly with concentration, ranging from 5.1 to 466.8 Pa. On the other hand, a decrease in the yield strain is observed when comparing the 5 wt% sample to the 7.5 and 10 wt% waxy model oils, from 3.04 to 0.62 %. The increase in yield stress implies that a more concentrated sample forms a stronger network. However, the material's strain capacity in the elastic regime is lower, making the network more

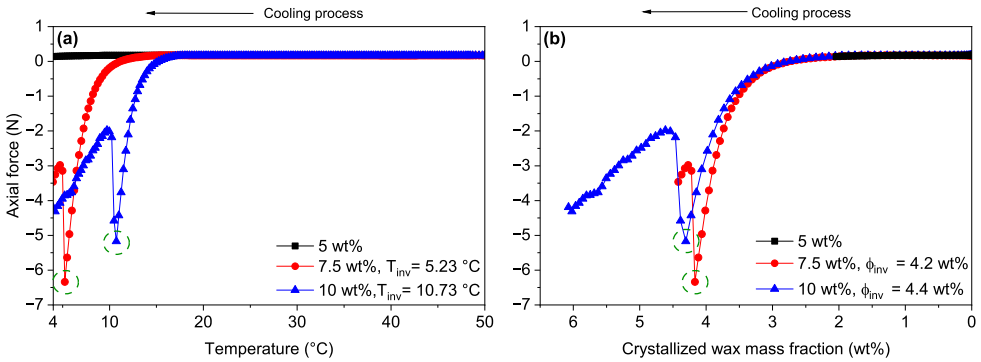


Fig. 12 Axial force variation during cooling for the samples containing 5, 7.5, and 10 wt% of wax at 1 °C·min^{-1} under 0.02 % of strain amplitude at 0.2 Hz with (a) temperature and (b) crystallized wax mass fraction. The green dashed line highlights the inversion points.

brittle. Nevertheless, the effect of the formed voids should not be undervalued in the breakage process.

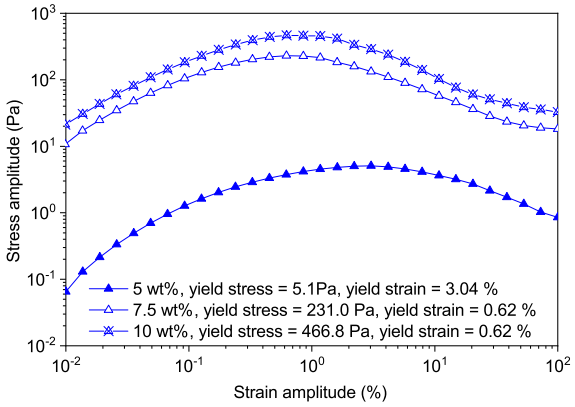


Fig. 13 Strain amplitude sweeps at 4 °C under 0.2 Hz for the samples containing 5, 7.5, and 10 wt% of wax and cooled at 1 °C·min^{-1}.

4.3.2 Effect of the cooling rate

Figure 14 shows the sample behavior under cooling for the 7.5 wt% waxy model oils at cooling rates of 0.5, 1, and 2 °C·min^{-1}, from (a) to (c), respectively. It is observed that the modulus crossover temperature decreases with the cooling rate. The values obtained were 15.6, 15, and 11.5 °C for the cooling rates of 0.5, 1, and 2 °C·min^{-1}, respectively. The results agree with the literature [3, 18]. In addition, the amount of crystallized wax necessary for gelation increases from 1.6 to 2.4 wt% in the range of 0.5 to 2 °C·min^{-1}. This fact may be attributed to different particle characteristics in size and number depending on the cooling rate [51, 52].

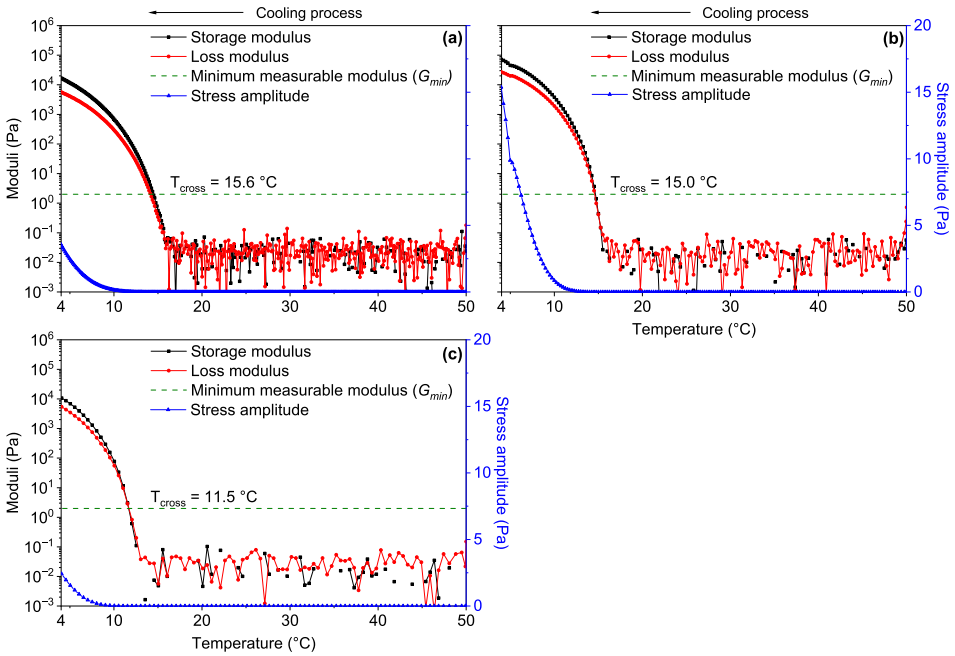


Fig. 14 Temperature ramp effect on moduli and stress amplitude for the 7.5 wt% samples cooled down at (a) 0.5, (b) 1, and (c) 2 °C·min^{-1}.

According to Figure 15, the amplitude sweep curves show that the cooling rate has a non-monotonic impact on the yield stress [51]. Comparing the rates of 0.5 and 1 °C·min^{-1}, there is an increase in the yield stress from 45.8 to 231 Pa. However, for the cooling rate of 2 °C·min^{-1}, an intermediate value of 102.8 Pa was obtained. The result corroborates the Andrade et al. [51] work, in which the rheological properties exhibited a non-monotonic behavior with the cooling rate. However, the validity of the observed behavior should be confirmed through repeatability tests, which will be addressed in the next section.

Regarding volume shrinkage, the samples did not exhibit visible void formation, and the kink during the cooling process was observed only at 1 °C·min^{-1} (T_{inv} = 5.23 °C and ϕ_{inv} = 4.2 wt%). Figure 16 shows the axial force behavior with temperature (a) and cooling rate (b). An inversion in the curves occurred only at 1 °C·min^{-1}. According to Pereira [53], the contraction of a model waxy oil, investigated by monitoring the sample edge in a parallel-plate geometry, revealed that contraction decreased as the cooling rate increased due to the thermal delay in sample heating.

4.3.3 Test repeatability

In the discussed experiments, the samples were prepared at 60 °C and tested over 3 weeks. Comparisons between samples with different elapsed times since preparation were not restricted. However, the same thermal history was ensured before each experiment. As shown in the repeatability tests for the 7.5 wt% sample in Figure 17, there is

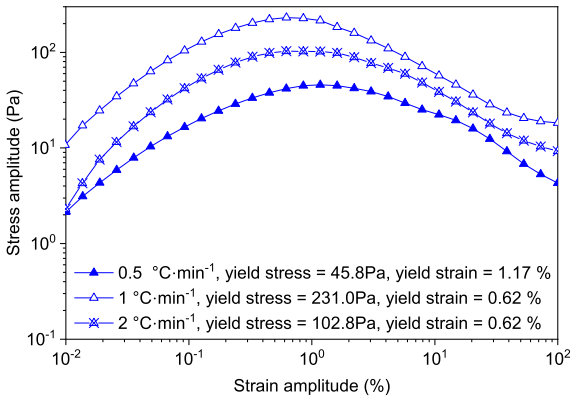


Fig. 15 Strain amplitude sweeps at 4 °C for the 7.5 wt% samples cooled down at 0.5, 1, and 2 °C·min^{-1}.

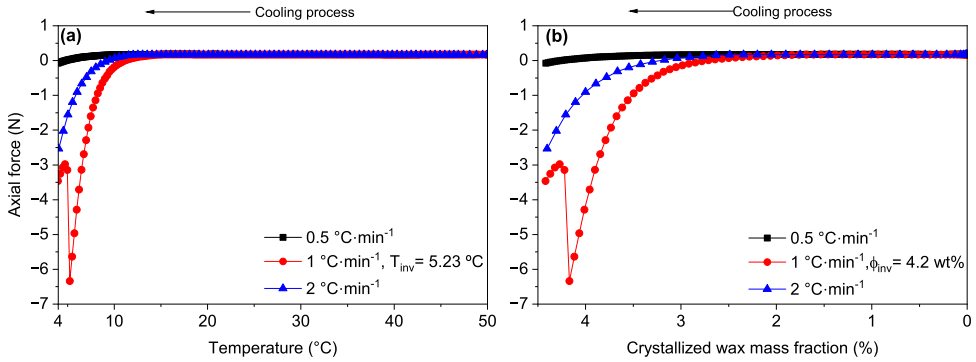


Fig. 16 Axial force variation during cooling for the 7.5 wt% samples cooled at 0.5, 1, and 2 °C·min^{-1} with (a) temperature (b) crystallized wax mass fraction.

a fourfold reduction in the yield stress when the samples from the first week and those tested in the third week after preparation are compared. Small volatile losses can be expected during this period. Nevertheless, sample evaporation increases the concentration of waxes by reducing the liquid phase, whereas the expected effect would be the opposite. Therefore, other factors may be responsible for this effect.

According to Andrade and Negrão [3], waxy model oils are less prone to thermal history effects when heated over the wax appearance temperature. However, long-term aging of the sample affected the rheology test results. In the next section, the effects of sample aging, sample preparation, and initial test temperature on axial force variation were systematically evaluated.

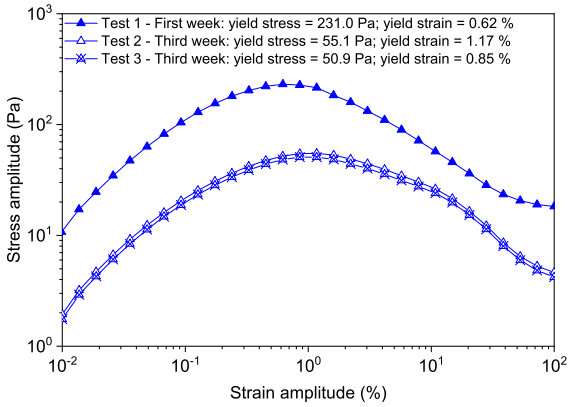


Fig. 17 Strain amplitude sweeps at 4 °C under 0.2 Hz for the 7.5 wt% samples cooled at 1 °C·min^{-1} in the first and third week after sample preparation.

4.4 Analysis of volume shrinkage-induced artifacts in grooved Couette geometry

4.4.1 Onset of cavity formation and local failure

As discussed in the previous section, the formation of voids was not visually observed in the 5 and 7.5 wt% waxy model oils. Moreover, the inflection in axial force did not occur in every test using 7.5 wt% samples. In this study, samples containing 8 and 9 wt% were also tested to determine the onset of void formation and compared with the concentrations of 7.5 and 10 wt%. Figure 18 shows the storage modulus and axial force behavior during cooling for 7.5, 8, 9, and 10 wt% at 1 °C·min^{-1} under oscillatory tests (0.02 % of strain amplitude and a frequency of 0.2 Hz). In Figure 18, T_{kink} represents the temperature at which the kink was observed in the storage modulus and T_{inv} the temperature at which the axial force inversion occurred.

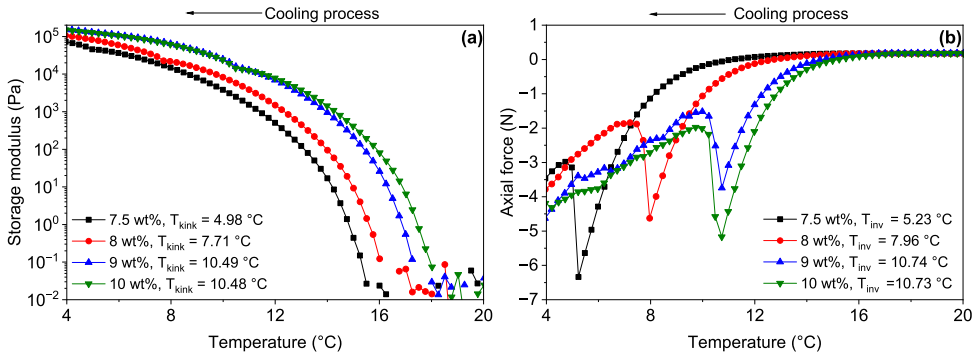


Fig. 18 Storage modulus (a) and axial force (b) during cooling for 7.5, 8, 9, and 10 wt% samples at 1 °C·min^{-1}, under 0.02 % of strain amplitude at 0.2 Hz.

Figure 18 (a) shows that all the samples displayed a kink in the storage modulus curves during cooling in the condition studied. Accordingly, Figure 18 (b) shows a strong decrease in axial force, marked by an abrupt inversion at a temperature close to T_{kink}. The difference between T_{inv} and T_{kink} was around 0.2 °C, which corresponds to a change in crystallized wax mass fraction of less than 0.1 wt%. Given this scenario, from 7.5 wt% volume shrinkage, related artifacts may occur in the samples. It should also be noted that for a fixed cooling rate, T_{kink} differs among samples by 0.2 wt% of crystallized wax, corresponding to 4.2 wt% for the 7.5 wt% sample and 4.4 wt% for the 10 wt% waxy model oil.

To relate axial force to storage modulus, a plot of the two variables using the data of Figure 18 was provided in Figure 19 (a). Moreover, Figure 19 (b) highlights the kink effect in the storage modulus (G') data through the G' derivative with temperature. Figure 19 (a) shows that the minimum axial force modulus observed in the curve inversion was 3.7 N for the 9 wt% sample and the maximum was 6.3 N for the 7.5 wt% sample. Furthermore, except for the 10 wt% sample, the general trend of the inversion artifact is that, by increasing the initial wax concentration, the inversion point occurs at a smaller axial force. Similarly, Figure 19 (b) shows that storage modulus derivatives display an abrupt jump due to the kink effect, which occurs at higher temperatures as the initial wax concentration is increased.

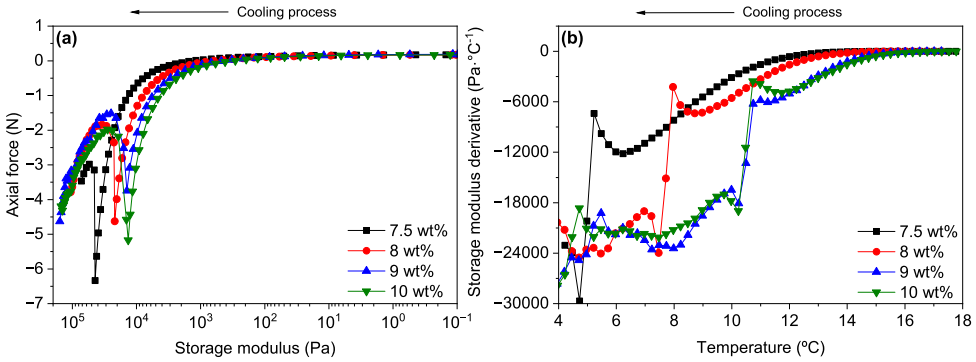


Fig. 19 (a) Axial force versus storage modulus and (b) storage modulus derivative with temperature for 7.5, 8, 9, and 10 wt% samples at 1 °C·min^{-1}, under 0.02 % of strain amplitude at 0.2 Hz.

Despite the axial force issues, the strain amplitude sweep tests did not show any particular artifact. In fact, the yield stress increased with concentration, as shown in Figure 20. The same trend was previously observed comparing 5, 7.5, and 10 wt% samples. From Figure 20 yield stresses of 231.0, 287.1, 449.0, and 466.8 Pa were measured for 7.5, 8, 9, and 10 wt%, respectively. Meanwhile, a yield strain of 0.62 was obtained for all concentrations. Similar results were also observed for hydrate slurries. Coelho et al. [54] observed that by increasing gas concentration in hydrate formation, yield stress increased, although yield strain remained fixed. Similar observations were made by Ferrari et al. [55] by increasing water cut in a cyclopentane hydrate slurry.

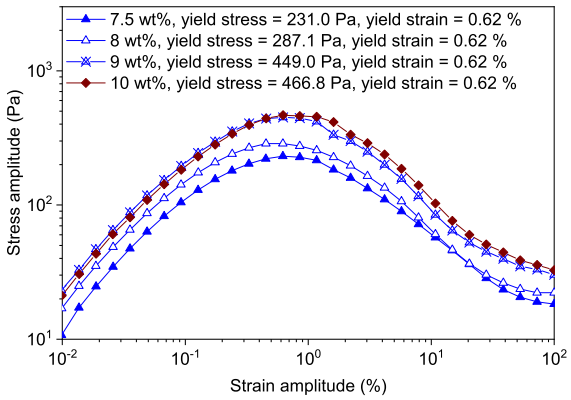


Fig. 20 Strain amplitude sweeps at 4 °C for 7.5, 8, 9, and 10 wt% samples cooled at 1 °C·min^{-1}, under 0.02 % of strain amplitude and 0.2 Hz.

To track cavity formation, a test using a 10 wt% waxy model oil was performed while the sample was recorded. The storage modulus and axial force behavior from 20 to 4 °C are shown in Figure 21 (a) and the strain amplitude sweep is depicted in Figure 21 (b). The inversion in the axial force curve and the kink in the storage modulus occurred around 8 °C. Furthermore, a yield stress of 220.8 Pa and a yield strain of 0.7 % were obtained.

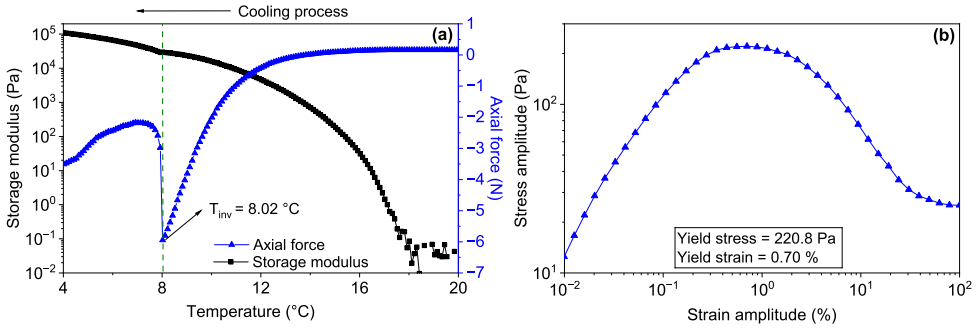


Fig. 21 Temperature ramps (a) and amplitude sweep (b) results for the recorded 10 wt% sample (0.02 of strain amplitude % and 1 Hz).

Simultaneously, the sample was recorded from 30 to 4 °C to observe the void formation, as shown in Figure 22. At 30 °C, there is no visual evidence of crystallization (Figure 22 (a)). As the temperature decreases and crystallization occurs, the sample becomes visually blurred and then completely opaque, as shown in Figure 22 (b) and (c). At 8 °C, it was observed that the void had not yet been formed, although an inversion in axial force behavior occurred. However, from this point, a slight change in the color is noted in the sample (Figure 22 (e)). The color change is followed by the sample's collapse into a cavity, as shown in Figure 22 (f), (g), and (h).

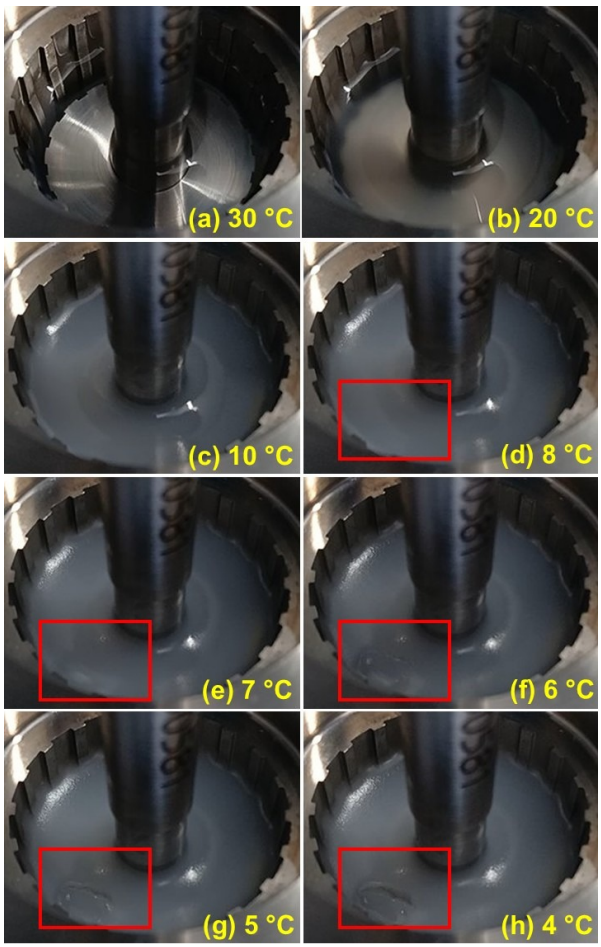


Fig. 22 Formation and evolution of the cavity in a grooved Couette geometry for a 10 wt% waxy model oil at 1 °C·min^{-1} under 0.02% at 1 Hz.

After cooling, the strain amplitude sweep was also performed. Figure 23 (a) and (b) show the sample before and after the test. The size of the cavity is about 6.3 mm, as revealed in Figure 23 (a). The amplitude sweep revealed a local failure between the bob and the cavity. The local failure region stands out from the circular pattern formed. More cavity pictures are available in Appendix D.

4.4.2 Sample aging at 4 °C

The mechanical behavior of the gel was monitored at 4 °C for 1 hour to evaluate potential aging effects. A small oscillatory perturbation of 0.02 % of strain amplitude was imposed at 0.2 Hz. The moduli and axial force behavior obtained during cooling and isothermal time are displayed in Figures 24 to 26 for 5.0. 7.5 and 10 wt% samples, respectively.

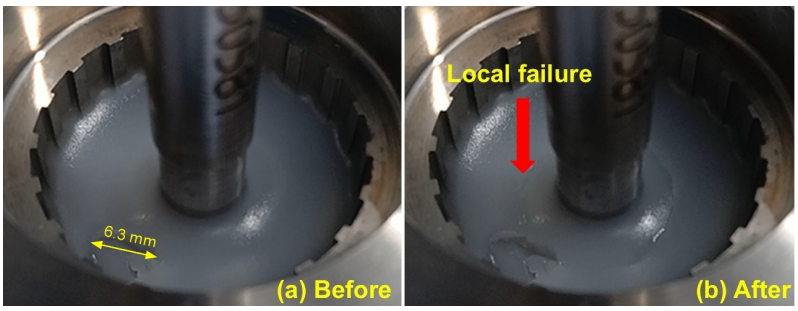


Fig. 23 Evidence of local failure in a 10 wt% waxy model oil (a) before and (b) after the strain amplitude sweep.

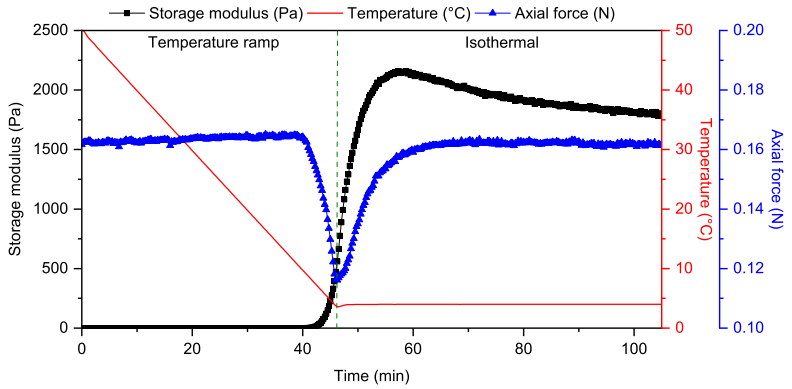


Fig. 24 Moduli and axial force behavior for a 5 wt% waxy model oil during the thermal protocol (0.02 % of strain amplitude at 0.2 Hz).

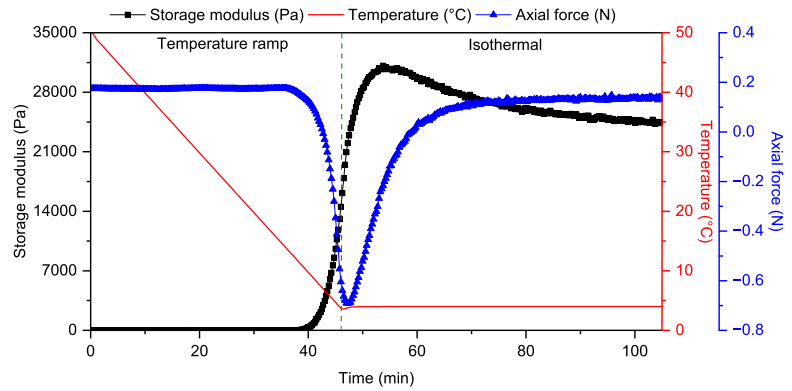


Fig. 25 Moduli and axial force behavior for a 7.5 wt% waxy model oil during the thermal protocol (0.02 % of strain amplitude at 0.2 Hz).

Figures 24 to 26 show that the storage modulus initially displays a significant growth after the material reaches 4 °C. However, after 10 to 15 minutes, the modulus

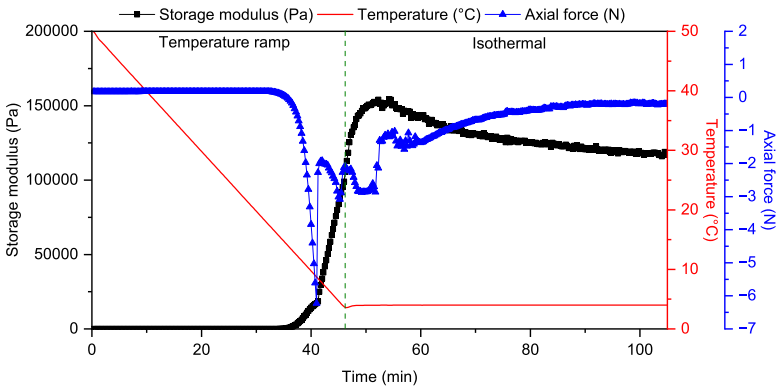


Fig. 26 Moduli and axial force behavior for a 10 wt% waxy model oil during the thermal protocol (0.02 % of strain amplitude at 0.2 Hz).

starts to decrease. The amount diminished relative to the maximum storage modulus observed, and the final points are approximately 16, 19, and 24 % for the 5, 7.5, and 10 wt% samples, respectively.

As discussed in the previous sections, during cooling, a decrease in the axial force was observed due to gelation [9, 20]. For the 5 wt% concentration, the variation in axial force was marginal. It did not significantly affect the test results in the Couette geometry, which was more robust at avoiding wall slip effects than the cone-and-plate sensor. However, after the cooling process, when the 5 and 7.5 wt% samples are kept at 4 °C, a stress relaxation effect is observed due to the increase in axial force (Figure 24 and 25). Since the material exerts a downward force on the bob, the gel may undergo network rearrangement when the cooling process is stopped. Moreover, sample detachment from the geometry is also expected, although in Couette geometry the bob is covered [9, 26]. Overall, the stress-relaxation phenomena led to non-monotonic behavior in the storage modulus. This effect is contrary to most results in the literature, which show that the hardening effect predominates over time [56, 57]. However, similar trends were reported by Mao et al. [26] and Shinde and Kumar [9]. In this scenario, it is important to highlight that the sample may be affected by multiple factors during aging. Ostwald ripening phenomena [56] and network rearrangement [58] are noteworthy. Residual crystallization was not observed at 4 °C under the experimental conditions applied in this work.

A different behavior was observed for the 10 wt% sample, as shown in Figure 26. For this sample, the formation of a cavity led to an abrupt inversion in the axial force slope signal yet during cooling. Moreover, at least three inversions in the curve signal are observed before stress relaxation occurs. Lastly, the results of the strain amplitude sweeps after the isothermal time are shown in Figure 27.

Figure 27 shows that the qualitative behavior of the stress amplitude curves is similar to the previous tests performed immediately after 4 °C. The yield stresses and strains obtained for 5, 7.5, and 10 wt% were 5.6, 60, and 310.6 Pa, and 3, 1.2, and 0.8 %, respectively. Overall, wall slip, stress relaxation, cavity formation, localized failures, and sample aging were highlighted for the samples studied. Note that the decreasing

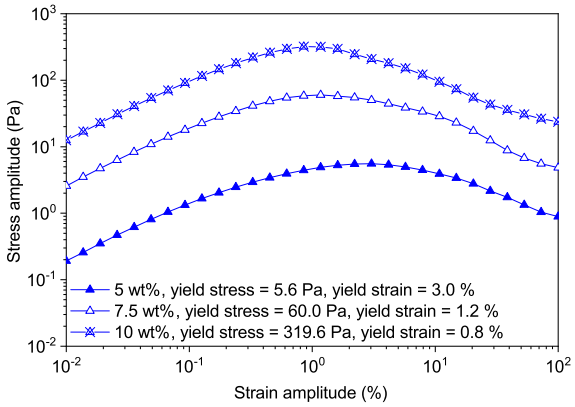


Fig. 27 Amplitude sweep after isothermal time under 0.2 Hz for (a) 5 wt%, (b) 7.5 wt%, and (c) 10 wt%.

yield strain trend with concentration differs from that of samples tested immediately at 4 °C.

4.4.3 Effect of the oscillation parameters

The previous section provided important results concerning the effects of wall slip and volume shrinkage. However, poor test repeatability was observed for 7.5 and 10 wt% samples, especially for the stress amplitude tests. The first source of error was the sample age after preparation. In addition, the test parameters were also evaluated for a 10 wt% sample as shown in Figure 28. The samples were tested within 3 days after preparation.

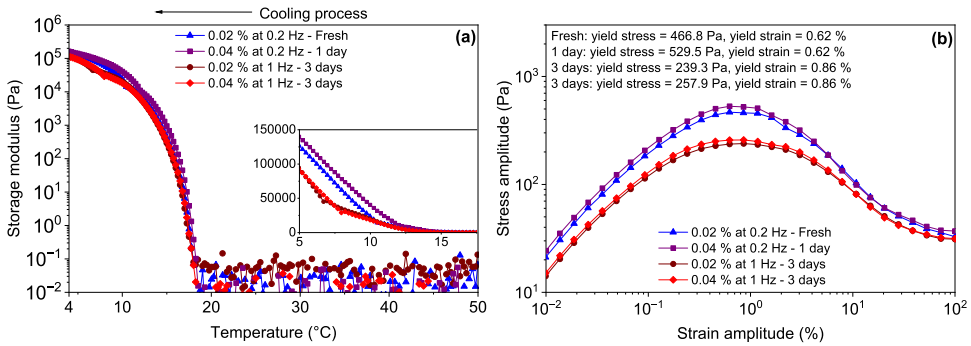


Fig. 28 (a) Storage modulus during cooling for a 10 wt% sample at 1 °C·min^{-1} and (b) strain amplitude sweep at 4 °C, under different oscillatory conditions.

According to Figure 28 (a), at 4 °C, the storage modulus achieved values of the order of 10^5. Furthermore, tests at 0.2 Hz led to higher storage modulus and yield stress values than at 1 Hz, as shown in Figure 28 (b). The yield stresses obtained were

466.8 and 529.5 Pa at 0.2 Hz for strain amplitudes of 0.02 and 0.04 %, respectively. At 1 Hz, values of 257.4 and 236.6 Pa for 0.02 and 0.04 % were measured. In addition, a yield strain of 0.62 % was obtained for 0.2 Hz and 0.86 % for 1 Hz. Upon initial inspection, it is observed that an increase in test frequency led to a reduction in yield stress. However, it can be noticed that the curves were grouped not only by frequency but also by sample age. The samples tested on the third day had smaller storage moduli and yield stresses at 4 °C. A similar trend was observed for the axial force behavior during cooling, as shown in Figure 29.

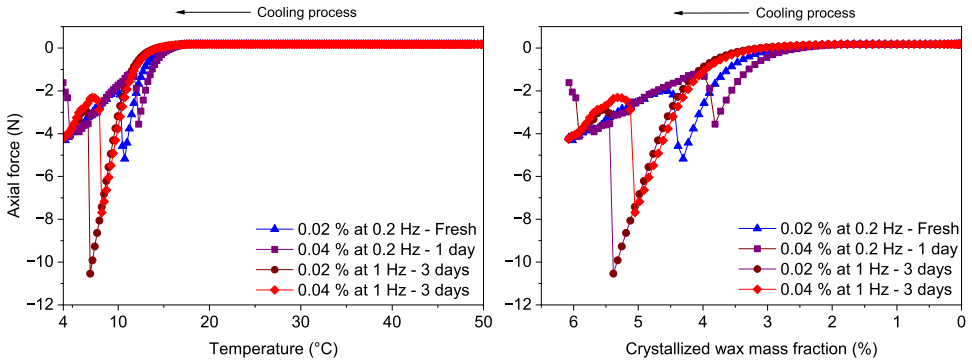


Fig. 29 Axial force behavior during cooling for a 10 wt% sample at 1 °C·min^{-1} with (a) temperature and (b) crystallized wax mass fraction.

In addition to the prior results, based on Figure 29, the samples tested at 0.2 Hz (fresh and 1-day samples) achieved axial forces more negative than those at 1 Hz (3-day samples). The difference was about twice. Therefore, the decrease in magnitude of the axial force is associated with lower yield stress values at 1 Hz. Moreover, Figure 29 compares the variation of axial force with temperature (a) and concentration (b). It is also important to notice that frequency also impacted kink temperatures in storage modulus curves and axial force inversions, as shown in Figure 29.

Overall, due to the fact that both frequency and sample age were varied simultaneously in the test, it was not possible to properly separate the effects of frequency and sample age from the results. For waxy oils, usually low frequencies with strain amplitudes in the linear viscoelastic region are preferred to minimize the impact of oscillations on the crystallization and gelation processes [15]. However, it is possible to increase the sampling interval and reduce stress-relaxation effects at 1 Hz.

4.4.4 Effect of the sample preparation temperature on the test repeatability

This study evaluated the effects of sample preparation temperature (T_P) and initial test temperature (T_0) on test results. A sample containing 10 wt% of wax was first investigated. Figures 30, 31, and 32 show the storage modulus curves during cooling, the strain amplitude sweep results, and the axial force behavior with temperature, respectively. Moreover, Table 6 displays a summary of the main results.

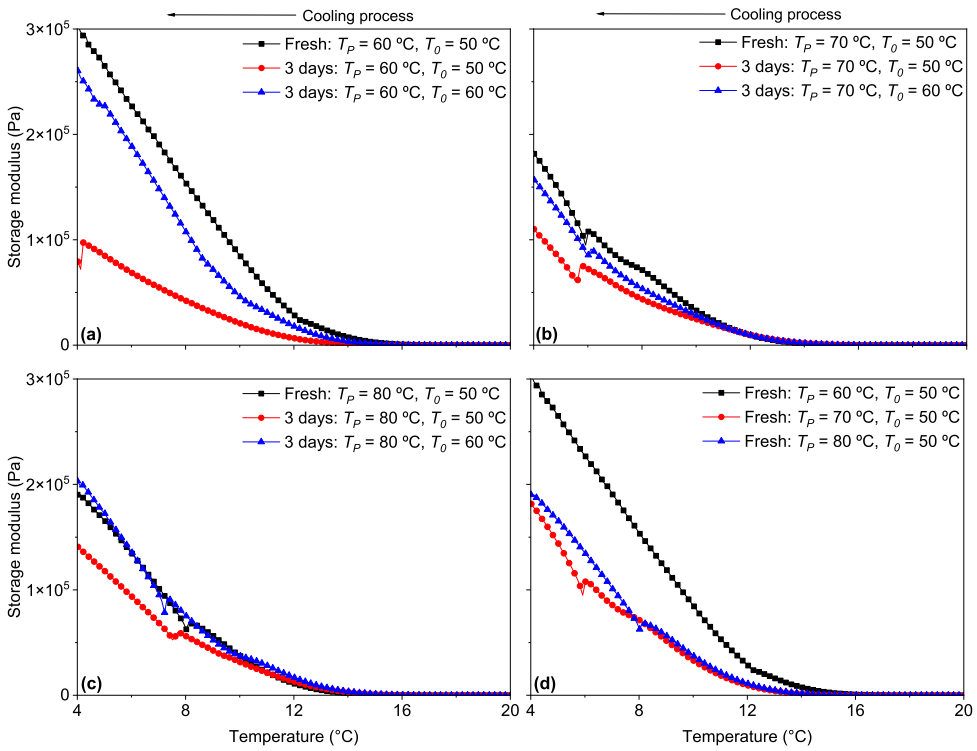


Fig. 30 Storage modulus during cooling for samples prepared at: (a) 60 ºC; (b) 70 ºC; (c) 80 ºC. (d) compares the different preparation temperatures. (10 wt% sample at 1 °C·min^{-1}; 0.02 % of strain amplitude at 1 Hz).

Figure 30 shows the storage modulus between 20 and 4°C for samples prepared at 60 °C (a), 70 °C (b), and 80 °C (c), for the fresh and 3-day samples. For 3-day samples, tests were conducted at 50 °C and 60 °C. Moreover, Figure 30 (d) compares the different initial temperatures for the fresh samples. Overall, the storage modulus curves indicate that similar gelation onsets occur across all experiments. However, the magnitude of the storage modulus at 4 °C is not the same, especially for the sample prepared at 60 °C (Figure 30 (a)). The differences between the modulus curves are less pronounced at 70 °C and 80 °C. Remarkably, the kink appearance temperatures on the storage modulus are also closer when the preparation temperature is increased. However, the storage modulus is lower for the 3-day sample compared with the fresh sample. Applying an initial temperature of 60 °C on the third day allowed recovery of the storage modulus values closer to those of the fresh sample. Therefore, in addition to the preparation temperature, the initial temperature also plays an important role in test repeatability. The storage modulus values at 4 °C (G'$_4$) are available in Table 6.

Based on Figure 31, it is observed that the differences between the stress peaks decrease as the preparation temperature is increased. In addition, results similar to those obtained by the fresh sample are obtained by increasing the initial temperature to 60 °C on the third day. Figure 31 (d) also shows very similar results to the stress

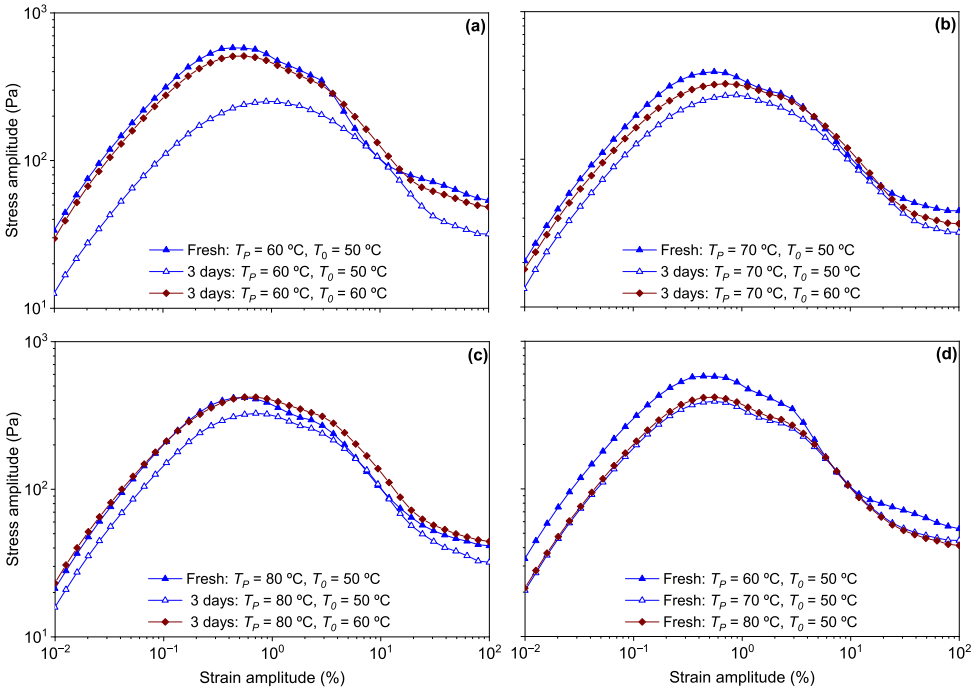


Fig. 31 Strain amplitude sweep at 4 °C at 1 Hz for samples prepared at: (a) 60 ºC; (b) 70 ºC; (c) 80 ºC. (d) compares the different preparation temperatures. (10 wt% sample cooled at 1 °C·min^{-1}).

curves of the fresh samples prepared at 70 and 80 °C, compared to the sample prepared at 60 °C. The yield stresses (τ_y) and strain (γ_y) are provided in Table 6. Recently, de Souza Cunha et al. [59] showed the impact of increasing initial test temperatures on the waxy oil yield stress. According to the authors, at temperatures slightly above the melting temperature of the wax, there is still persistence of molecular clusters that may act as nucleation sites.

According to Figure 32, the preparation temperature also impacts the axial force behavior. For the sample prepared at 60 °C (a), the onset of the axial force decrease (T_{on,F_N}), the minimum axial force ($F_{N,min}$), and the axial force inversion temperature are strongly affected by the sample age and initial temperature. At the preparation temperatures of 70 °C (b) and 80 °C (c), the properties are less affected by the sample age. However, the samples prepared at 70 °C (b) provided the best repeatability results for axial force. Moreover, by comparing only the results for the fresh sample, the increase in the preparation temperature impacted $F_{N,min}$ non-monotonically (d).

In general, in the presence of cavities, the repeatability and properties of tests were shown to be strongly dependent on preparation, initial temperature, and sample age. This result can be attributed to the random nature of cavity formation, which remains to be further elucidated (c.f. Appendix D). In this regard, a 7.5 wt% sample, free of visual cavity formation, was also tested and evaluated using a temperature ramp, an isothermal time at 4 °C, and a strain amplitude sweep. The sample was prepared at

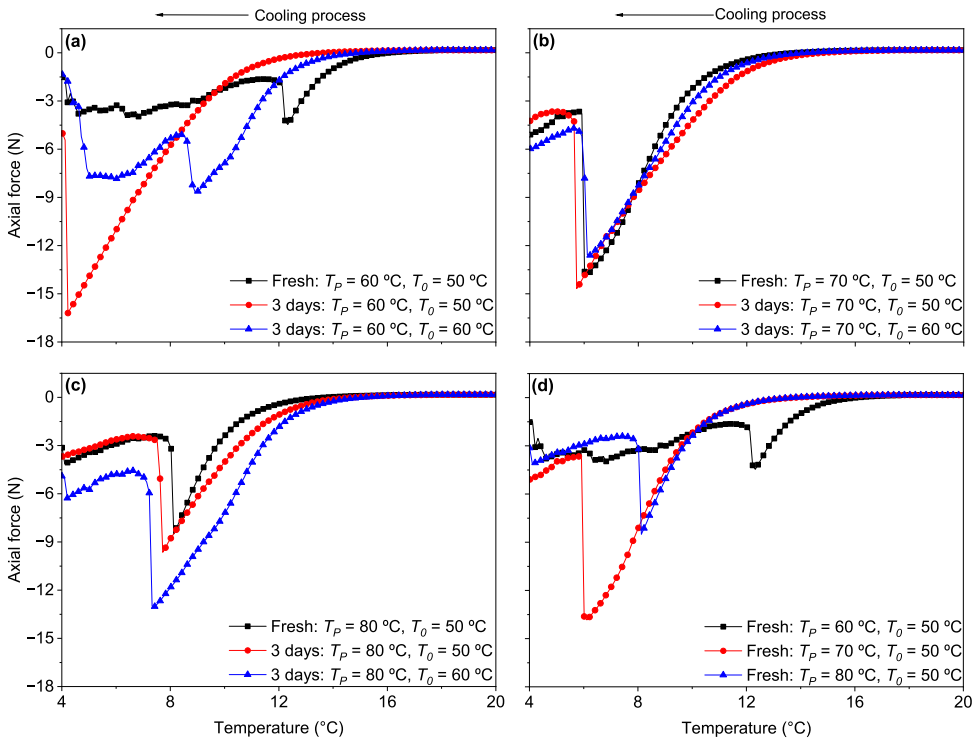


Fig. 32 Axial force during cooling for samples prepared at: (a) 60 ºC; (b) 70 ºC; (c) 80 ºC. (d) compares the different preparation temperatures. (10 wt% sample at 1 °C·min^{-1}; 0.02 % of strain amplitude at 1 Hz).

80 °C and tested fresh after 3 and 7 days. The storage modulus, axial force, and strain amplitude sweep results are shown in Figures 33 to 35.

Table 6 Sample properties dependence on preparation and initial temperature, T_P and T_0.

T_p(°C)	T_0(°C)	Age	τ_y(Pa)	γ_y(%)	G'$_4$(kPa)	$F_{N,min}$(N)	T_{on,F_N}(°C)
60	50	Fresh	579.6	0.44	304.2	-4.6	15.1
60	50	3 days	251.6	0.89	79.3	-16.2	10.5
60	60	3 days	510.2	0.56	260.3	-8.7	12.5
70	50	Fresh	391.3	0.56	181.6	-13.8	10.5
70	50	3 days	272.2	0.89	110.1	-14.7	11.7
70	60	3 days	324.6	0.71	156.6	-12.6	11.4
80	50	Fresh	418.5	0.56	190.3	-8.5	10.9
80	50	3 days	326.2	0.71	140.8	-9.6	11.9
80	60	3 days	420.9	0.71	203.3	-13.0	13.1

The curves in Figure 33 depict the increase in the storage modulus due to sample age, in contrast to the results observed for the 10 wt% sample. Yet, the properties

display the same qualitative non-monotonic behavior. It is important to note that the 7.5 wt% samples did not form cavities at the top of the material in this geometry.

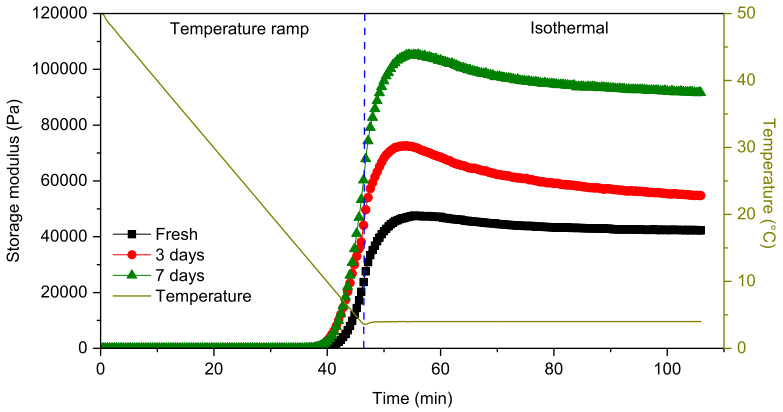


Fig. 33 Storage modulus during cooling and isothermal time for a 7.5 wt% sample at 1 °C·min^{-1}, fresh, and after 3 and 7 days of preparation (0.02 % of strain amplitude at 1 Hz).

A similar trend of increase in the properties is observed for the yield stress and yield strain, as shown in Figure 34. A possible cause for this growth is sample evaporation over the days. The reduction in the oil phase increases the ratio between the solid and liquid phases in the model oil. Small increases in concentration can strongly impact the rheological properties [18].

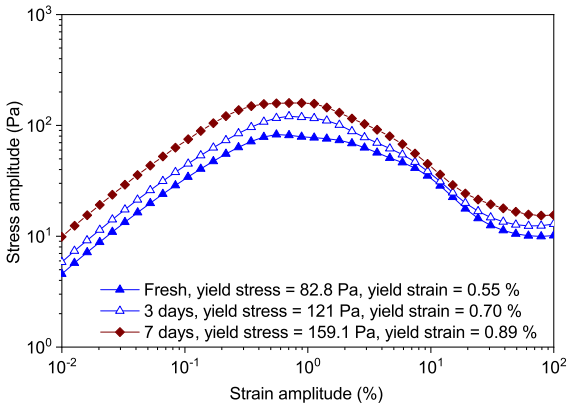


Fig. 34 Strain amplitude sweep after 1 hour at 4 °C for a 7.5 wt% sample cooled at 1 °C·min^{-1} under 1 Hz, for fresh, 3-day, and 7-day samples.

Lastly, Figure 35 shows a remarkable decrease in the axial force magnitude from the fresh sample to the 3-day and 7-day samples. For the 3-day sample, an abrupt

inversion of the curve was observed before it reached 4 °C. For the 7-day sample, the inversion smoothly occurred during the isothermal time.

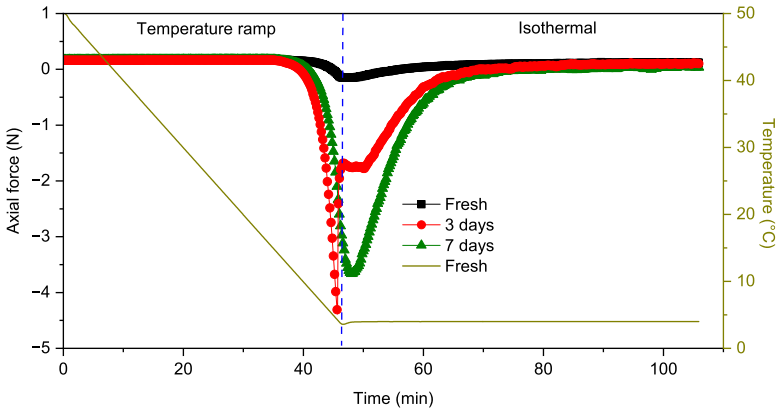


Fig. 35 Axial force during cooling and isothermal time for a 7.5 wt% sample at 1 °C·min^{-1}, fresh, and after 3 and 7 days of preparation (0.02 % of strain amplitude at 1 Hz).

Based on the evidence, several artifacts can emerge from sample volume shrinkage and cavity formation in grooved Couette geometries. Factors such as sample age, preparation temperature, and initial temperature can affect the properties non-monotonically. In this scenario, evaluating the axial force proved an efficient tool for identifying the artifacts. However, methods to address this limitation are still needed.

4.4.5 Non-monotonic storage modulus behavior in parallel plate geometry

The axial force behavior of the material was also investigated in a serrated 75 mm parallel plate geometry. Figure 36 shows the axial force behavior of the pure oil and 7.5 wt% samples during quiescent cooling at 1 °C·min^{-1}.

As for cone and plate geometry, in the parallel plates, the sample displays a small negative axial force value after sample loading, as shown in Figure 36. Similarly, the axial force decreases during cooling due to thermal contraction for the pure and model oils. However, for 7.5 wt% the axial force falls due to volume shrinkage effects caused by gelation. After approximately 4 min at 4 °C, the normal force reaches a minimum and then increases, indicating stress relaxation. The behavior was similar to the grooved Couette geometry. Nonetheless, for the grooved Couette geometry, after 1 hour, the axial force approached the initial value close to zero. For the parallel plates, the relaxation recovery after 1 hour was about 50 %.

Subsequently, the sample was tested under oscillation as shown in Figure 37.

Figure 37 shows that the minimum normal force achieved under oscillation was about double compared to the quiescent test. Due to stress relaxation, the same non-monotonic behavior of the storage modulus was also observed compared to the Couette geometry.

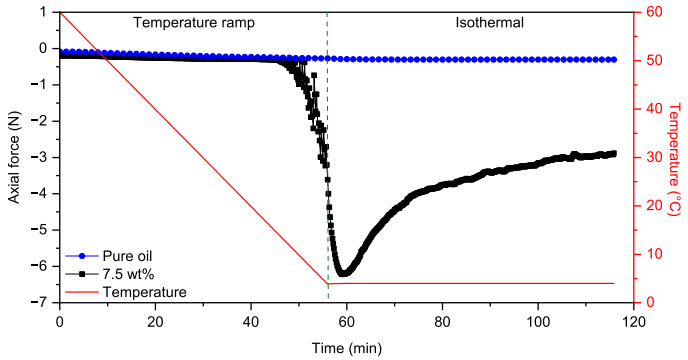


Fig. 36 Axial force behavior for fixed gap condition during quiescent cooling and isothermal time for the pure oil and a 7.5 wt% sample at 1 °C·min^{-1}.

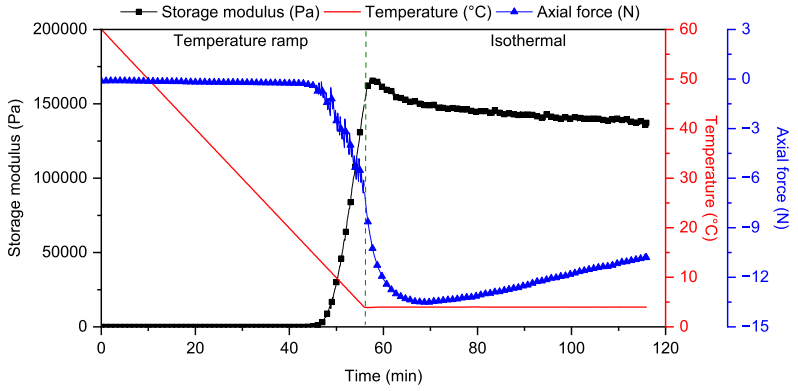


Fig. 37 Storage modulus and axial force behavior during cooling and isothermal time for a 7.5 wt% sample at 1 °C·min^{-1} under constant gap (0.02 % of strain amplitude at 1 Hz).

Figure 38 shows how the sample behaves during breakage, when it is cooled quiescently using a constant gap. According to Figure 38, there was an abrupt decrease in stress after the curve achieved the peak for the quiescent cooling. This effect can result from wall slip due to the strong downward force acting on the geometry.

In light of the results obtained, performing normal force-controlled tests can help prevent wall slip and volume shrinkage artifacts. However, it should be noted that the test is not fully quiescent, as the sample is compressed to compensate for volume shrinkage. Besides, the normal force control during the tests can hinder the natural normal force effects characteristic of the sample. In this regard, under quiescent cooling, the normal force should be controlled only until shrinkage and relaxation effects have ended, and then the test should be performed. When properties are measured during cooling, it is worth measuring beforehand and then providing the gap profile needed to compensate for volume shrinkage during the test.

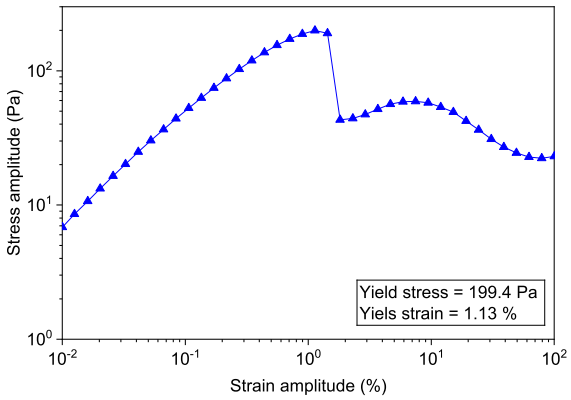


Fig. 38 Strain amplitude sweep under 1 Hz after the isothermal time at 4 °C for fixed gap and fixed normal force protocols.

5 Conclusion

In this work, wall-slip and volume shrinkage artifacts were evaluated in waxy model oils during oscillatory rheological tests. Sandblasted cone-and-plate geometries were shown to be more prone to wall slip than grooved concentric cylinders (GCC), as evidenced by abrupt changes and data scattering in the rheological tests. In this scenario, the occurrence of wall-slip is intensified by sample volume shrinkage, which, combined with the gelation process, decreases the axial force during cooling. As a result, the geometry rotor is pulled downward and facilitates sample detachment. This effect is less pronounced in the concentric cylinder geometry because the sample distribution within the geometry covers the bob. However, for concentrations of 8 to 10 wt%, GCC geometry also had a strong effect on the reduction in axial force during cooling in the test results. Among the artifacts, it was observed:

- Formation of localized cavities on the sample, which implies the presence of kinks in the rheological data. This effect occurs together with an inversion in the axial force growth. In addition, during breakage, a localized fracture of the sample was observed, as evidenced by images.
- Non-monotonic behavior of the storage modulus during sample aging in grooved Couette and parallel plate geometries, which peaked and displayed successive decreases over time. This behavior was accompanied by a stress relaxation effect due to sample detachment and rearrangement.
- Poor test repeatability and strong dependence of preparation temperature, initial test temperature, and sample age on test results. In general, increasing the preparation temperature and the initial test temperature improved test repeatability.

Future work may focus on using test strategies to compensate for volume shrinkage and obtain more accurate data, as well as on establishing proper protocols for sample preparation and initial test temperatures.

Supplementary information. Available.

Acknowledgments. The authors acknowledge Professor Kristofer Paso, the Ugelstad Laboratory, and the NTNU Chemical Engineering Department for providing the facilities and support to conduct this research. The authors also thank the Coordenação de Aperfeiçoamento de Pessoal de Nível Superior - Brasil (CAPES) - Finance Code 001, and the Conselho Nacional de Desenvolvimento Científico e Tecnológico - Brazil (CNPq) for the support.

Declarations

Funding. The authors declare funding from the Coordenação de Aperfeiçoamento de Pessoal de Nível Superior - Brasil (CAPES) - Finance Code 001, from the Conselho Nacional de Desenvolvimento Científico e Tecnológico - Brasil (CNPq), and from the NTNU Chemical Engineering Department (IKP) to cover lab leasing expenses.

Conflict of interest/Competing interests. The authors declare no conflict of interest.

Ethics approval and consent to participate. Not applicable.

Consent for publication. Not applicable.

Data availability. Data availability on request.

Materials availability. Not applicable.

Code availability. Not Applicable.

Author contribution. **André da Silva Guimarães:** conceptualization, methodology, formal analysis, investigation, and original draft. **Thiago Oliveira Marinho:** conceptualization, formal analysis, review and editing, and supervision. **Pedro Tavares Pereira:** conceptualization, formal analysis, and original draft. **Príamo Albuquerque Melo:** conceptualization, formal analysis, review and editing, and supervision. **Roney Leon Thompson:** conceptualization, formal analysis, review and editing, and supervision. **Márcio Nele:** conceptualization, formal analysis, review and editing, and supervision.

References

[1] Rønningsen, H.P.: Rheological behaviour of gelled, waxy north sea crude oils. Journal of Petroleum Science and Engineering **7**(3-4), 177–213 (1992)

[2] Visintin, R.F., Lapasin, R., Vignati, E., D'Antona, P., Lockhart, T.P.: Rheological behavior and structural interpretation of waxy crude oil gels. Langmuir **21**(14), 6240–6249 (2005)

[3] Andrade, D.E., Negrão, C.O.: Rheology of waxy oils: A critical review. Applications in Engineering Science **21**, 100202 (2024)

[4] Venkatesan, R., Nagarajan, N., Paso, K., Yi, Y.-B., Sastry, A., Fogler, H.: The strength of paraffin gels formed under static and flow conditions. Chemical Engineering Science **60**(13), 3587–3598 (2005)

[5] Huang, Z., Lee, H.S., Senra, M., Scott Fogler, H.: A fundamental model of wax deposition in subsea oil pipelines. AIChE Journal **57**(11), 2955–2964 (2011)

[6] Van Der Geest, C., Guersoni, V.C.B., Bannwart, A.C.: Experimental study of the time to restart the flow of a gelled waxy crude in rheometer and pipeline. Journal of Petroleum Science and Engineering **181**, 106247 (2019)

[7] Geri, M., Venkatesan, R., Sambath, K., McKinley, G.H.: Thermokinematic memory and the thixotropic elasto-viscoplasticity of waxy crude oils. Journal of Rheology **61**(3), 427–454 (2017)

[8] Marinho, T.O., Marchesini, F.H., Oliveira, M.C., Nele, M.: Apparent wall slip effects on rheometric measurements of waxy gels. Journal of Rheology **65**(2), 257–272 (2021)

[9] Shinde, S.B., Kumar, L.: Influence of the thermal shrinkage-induced volume contraction on the yielding behavior of waxy oil. Journal of Rheology **68**(4), 603–622 (2024)

[10] Ventura, V.F., Guimarães, A.S., Motta, A.B., Souza, M.N., Mitre, J.F., Thompson, R.L.: A numerical investigation on the influence of temperature and cooling rate in the restart problem of waxy crude oils in pipelines. Journal of Non-Newtonian Fluid Mechanics **349**, 105625 (2026)

[11] Ewoldt, R.H., Johnston, M.T., Caretta, L.M.: Experimental challenges of shear rheology: How to avoid bad data. In: Spagnolie, S.E. (ed.) Complex Fluids in Biological Systems: Experiment, Theory, and Computation, pp. 207–241. Springer, New York (2015)

[12] Marchesini, F.H., Alicke, A.A., Souza Mendes, P.R., Ziglio, C.M.: Rheological characterization of waxy crude oils: Sample preparation. Energy & Fuels **26**(5), 2566–2577 (2012)

[13] Andrade, D.E., Ferrari, M., Coussot, P.: The liquid regime of waxy oils suspensions: A magnetic resonance velocimetry analysis. Journal of Non-Newtonian Fluid Mechanics **279**, 104261 (2020)

[14] Zhao, Y., Paso, K., Sjöblom, J.: Thermal behavior and solid fraction dependent gel strength model of waxy oils. Journal of Thermal Analysis and Calorimetry **117**, 403–411 (2014)

[15] Marinho, T.O., Barbato, C.N., Freitas, G.B., Duncke, A.C., Oliveira, M.C., Nele, M.: Interaction effects of predominantly linear and branched waxes on yield stress

and elastic modulus of waxy oils. Energy & Fuels **32**(8), 8057–8068 (2018)

[16] Freitas, G.B., Duncke, A.C., Barbato, C.N., Oliveira, M.C., Pinto, J.C., Nele, M.: Influence of wax chemical structure on W/O emulsion rheology and stability. Colloids and Surfaces A: Physicochemical and Engineering Aspects **558**, 45–56 (2018)

[17] Marinho, T.O., De Oliveira, M.C., Nele, M.: Experimental investigation of the rheology and crystal morphology of model waxy oils under gelling conditions. Energy & Fuels **33**(10), 9604–9618 (2019)

[18] Guimarães, A.S., Marinho, T.O., Melo, P.A., Thompson, R.L., Oliveira, M.C., Nele, M.: Prediction of yield stress of waxy gels in pipelines using scaling theory and crystallization kinetics. Geoenergy Science and Engineering **226**, 211791 (2023)

[19] Paso, K., Senra, M., Yi, Y., Sastry, A., Fogler, H.S.: Paraffin polydispersity facilitates mechanical gelation. Industrial & engineering Chemistry Research **44**(18), 7242–7254 (2005)

[20] Shinde, S.B., Kumar, L.: New method for gelation temperature measurement without disturbing the crystal network. Industrial & Engineering Chemistry Research **60**(23), 8565–8578 (2021)

[21] Rodriguez-Fabia, S., Lopez Fyllingsnes, R., Winter-Hjelm, N., Norrman, J., Paso, K.G.: Influence of measuring geometry on rheomalaxis of macrocrystalline wax–oil gels: alteration of breakage mechanism from adhesive to cohesive. Energy & Fuels **33**(2), 654–664 (2019)

[22] Harris, C.G., Rice, C.E., Shetty, A., Mahir, L., Larson, R.G.: Precipitated wax content and yield stress of model wax-oil mixtures determined by arrest of flow during cooling at fixed stress. Journal of Rheology **67**(6), 1073–1089 (2023)

[23] Lee, H.S., Singh, P., Thomason, W.H., Fogler, H.S.: Waxy oil gel breaking mechanisms: adhesive versus cohesive failure. Energy & Fuels **22**(1), 480–487 (2008)

[24] Palermo, T., Tournis, E.: Viscosity prediction of waxy oils: Suspension of fractal aggregates (SoFA) model. Industrial & Engineering Chemistry Research **54**(16), 4526–4534 (2015)

[25] Haider, M., Hubert, P., Lessard, L.: Cure shrinkage characterization and modeling of a polyester resin containing low profile additives. Composites Part A: Applied Science and Manufacturing **38**(3), 994–1009 (2007)

[26] Mao, B., Divoux, T., Snabre, P.: Normal force controlled rheology applied to agar gelation. Journal of Rheology **60**(3), 473–489 (2016)

[27] Khoun, L., Hubert, P.: Cure shrinkage characterization of an epoxy resin system by two in situ measurement methods. Polymer composites **31**(9), 1603–1610 (2010)

[28] Abedi, B., C Rodrigues, E., Souza Mendes, P.R.: Irreversible time dependence of gelled waxy crude oils: Flow experiments and modeling. Journal of rheology **64**(5), 1237–1250 (2020)

[29] Abedi, B., Miguel, M.J.P., Souza Mendes, P.R., Mendes, R.: Startup flow of gelled waxy crude oils in pipelines: The role of volume shrinkage. Fuel **288**, 119726 (2021)

[30] Chala, G.T., Sulaiman, S.A., Japper-Jaafar, A.: Flow start-up and transportation of waxy crude oil in pipelines-a review. Journal of Non-Newtonian Fluid Mechanics **251**, 69–87 (2018)

[31] Phillips, D.A., Forsdyke, I.N., McCracken, I.R., Ravenscroft, P.D.: Novel approaches to waxy crude restart: Part 1: Thermal shrinkage of waxy crude oil and the impact for pipeline restart. Journal of Petroleum Science and Engineering **77**(3-4), 237–253 (2011)

[32] Chala, G.T., Sulaiman, S.A., Japper-Jaafar, A., Abdullah, W.A.K.W., Mokhtar, M.M.M.: Gas void formation in statically cooled waxy crude oil. International Journal of Thermal Sciences **86**, 41–47 (2014)

[33] Chala, G.T., Sulaiman, S.A., Japper-Jaafar, A., Abdullah, W.A.K.W.: Effects of cooling regime on the formation of voids in statically cooled waxy crude oil. International Journal of Multiphase Flow **77**, 187–195 (2015)

[34] Chala, G.T., Sulaiman, S.A., Japper-Jaafar, A., Abdullah, W.A.K.W.: Study on influence of flow rates on voids in waxy crude oil subjected to dynamic and static cooling. Journal of Mechanical Engineering and Sciences **9**, 1587–1594 (2015)

[35] Chala, G.T., Sulaiman, S.A., Japper-Jaafar, A., Abdullah, W.A.K.W.: Investigation of convective heat transfer coefficient and initial temperature of waxy crude oil on the formation of voids. International Journal of Automotive and Mechanical Engineering **13**(3), 3754–3762 (2016)

[36] Chala, G.T., Sulaiman, S.A., Japper-Jaafar, A., Abdullah, W.A.K.W.: Temporal variation of voids in waxy crude oil gel in the presence of temperature gradient. Chemical Engineering Communications **207**(10), 1403–1414 (2020)

[37] Chen, J., Zhang, J., Li, H.: Determining the wax content of crude oils by using differential scanning calorimetry. Thermochimica Acta **410**(1-2), 23–26 (2004)

[38] Chala, G.T., Sulaiman, S.A.: Voids size distribution in gelled waxy crude oil under dynamic and static cooling. Petroleum Research **9**(1), 109–114 (2024)

[39] Huang, Z., Wang, B., Li, H.: Application of electrical capacitance tomography to the void fraction measurement of two-phase flow. IEEE Transactions on Instrumentation and Measurement **52**(1), 7–12 (2003)

[40] Shafquet, A., Ismail, I., Jaafar, A.: Thermal effect on void formation of waxy crude oil using electrical capacitance tomography. Jurnal Teknologi (Sciences & Engineering) **63**(1) (2013)

[41] Shafquet, A., Ismail, I., Jaafar, A.: Application of electrical capacitance tomography on single-plane sensor measurement. In: 2013 IEEE International Conference on Smart Instrumentation, Measurement and Applications (ICSIMA), pp. 1–5 (2013). IEEE

[42] Shafquet, A., Ismail, I., Japper-Jaafar, A., Sulaiman, S.A., Chala, G.T.: Estimation of gas void formation in statically cooled waxy crude oil using online capacitance measurement. International Journal of Multiphase Flow **75**, 257–266 (2015)

[43] Nascimento Wrasse, A., Santos, E.N., Silva, M.J., Wu, H., Tan, C.: Capacitive sensors for multiphase flow measurement: A review. IEEE Sensors Journal **22**(22), 21391–21409 (2022)

[44] Rostron, P.: Critical review of pipeline scale measurement technologies. Indian Journal of Science and Technology **11**(17), 1–18 (2018)

[45] Dimitriou, C.J., McKinley, G.H., Venkatesan, R.: Rheo-piv analysis of the yielding and flow of model waxy crude oils. Energy & Fuels **25**(7), 3040–3052 (2011)

[46] Macosko, C.W.: Rheology: Principles, Measurements, and Applications. Wiley-VCH, New York (1994)

[47] Japper-Jaafar, A., Bhaskoro, P., Sean, L., Sariman, M., Nugroho, H.: Yield stress measurement of gelled waxy crude oil: Gap size requirement. Journal of Non-Newtonian Fluid Mechanics **218**, 71–82 (2015)

[48] Ruwoldt, J., Sørland, G.H., Simon, S., Oschmann, H.-J., Sjöblom, J.: Inhibitor-wax interactions and PPD effect on wax crystallization: New approaches for GC/MS and NMR, and comparison with DSC, CPM, and rheometry. Journal of Petroleum Science and Engineering **177**, 53–68 (2019)

[49] Savasdipol, A., Paradee, N., Niamlang, S.: The recovery process of used hydrocarbon solvent by vacuum distillation. In: IOP Conference Series: Materials Science and Engineering, vol. 559, p. 012018 (2019). IOP Publishing

[50] Davies, A.N.: The new automated mass spectrometry deconvolution and identification system (AMDIS). Spectroscopy Europe **10**(3), 22–26 (1998)

[51] Andrade, D.E., Neto, M.A.M., Negrão, C.O.: Non-monotonic response of waxy oil gel strength to cooling rate. Rheologica Acta **57**(10), 673–680 (2018)

[52] Guimarães, A.S., Marinho, T.O., Melo, P.A., Oliveira, M.C.K.d., Thompson, R.L., Nele, M.: Image processing and analysis for fractal dimension and lacunarity calculation of waxy oil gels using polarized light micrographs. Crystal Growth & Design **24**(17), 7031–7043 (2024)

[53] Pereira, P.T.: Estudo da contração térmica e formação de vazios na garantia de escoamento de petróleos parafínicos. Bachelor's thesis in Chemical Engineering, Universidade Federal do Rio de Janeiro, Rio de Janeiro (2025)

[54] Coelho, I., Soares, E.J., Thompson, R.L., Pereira, F.d.A.R., Teixeira, A., Valim, L.S.: Rheological characterization and formation protocol of tetrahydrofuran hydrate slurries. Energy & Fuels **36**(15), 8538–8551 (2022)

[55] Ferrari, W., Soares, E.J., Thompson, R.L., Pereira, F.A., Siqueira, R.N., Teixeira, A., Valim, L.S.: Rheological characterization of cyclopentane hydrate slurries. Brazilian Journal of Chemical Engineering, 1–11 (2026)

[56] Coutinho, J.A., Silva, J., Ferreira, A., Rosário Soares, M., Daridon, J.-L.: Evidence for the aging of wax deposits in crude oils by ostwald ripening. Petroleum science and technology **21**(3-4), 381–391 (2003)

[57] Henaut, I., Betro, B., Vinay, G.: Differential scanning calorimetry contribution to a better understanding of the aging of gelled waxy crude oils. Oil & Gas Science and Technology–Revue d'IFP Energies nouvelles **74**, 16 (2019)

[58] Lazzari, S., Nicoud, L., Jaquet, B., Lattuada, M., Morbidelli, M.: Fractal-like structures in colloid science. Advances in colloid and interface science **235**, 1–13 (2016)

[59] Souza Cunha, M., Andrade, D.E., Soares, J.E.: The role of initial temperature on the yield stress of formulated waxy oils. Rheologica Acta **65**, 867–877 (2026)

Supplementary Files

This is a list of supplementary files associated with this preprint. Click to download.

- Supplementarymaterial.pdf